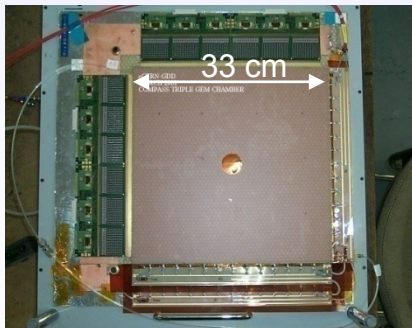
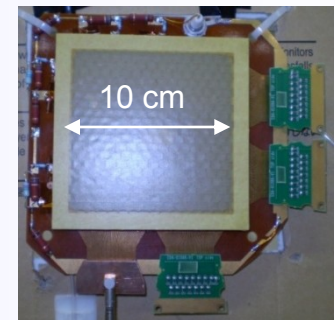
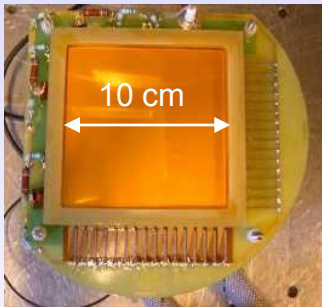


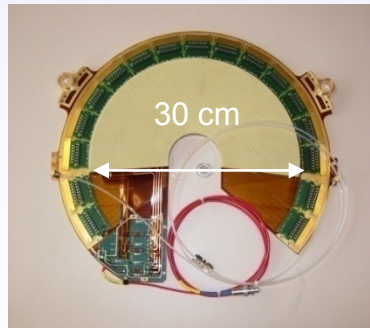
Gaseous Detectors

Introduction

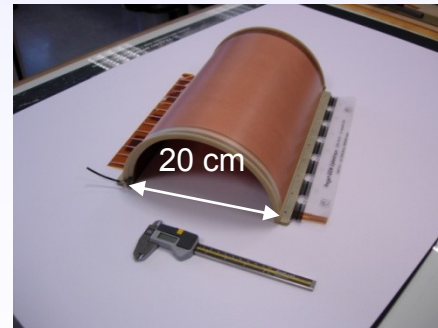
Leszek Ropelewski CERN-PH-DT



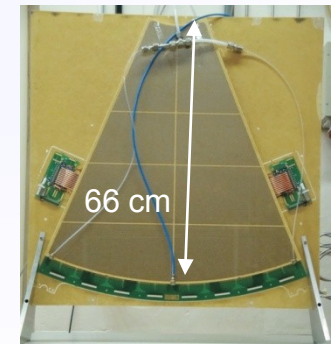
Compass



Totem



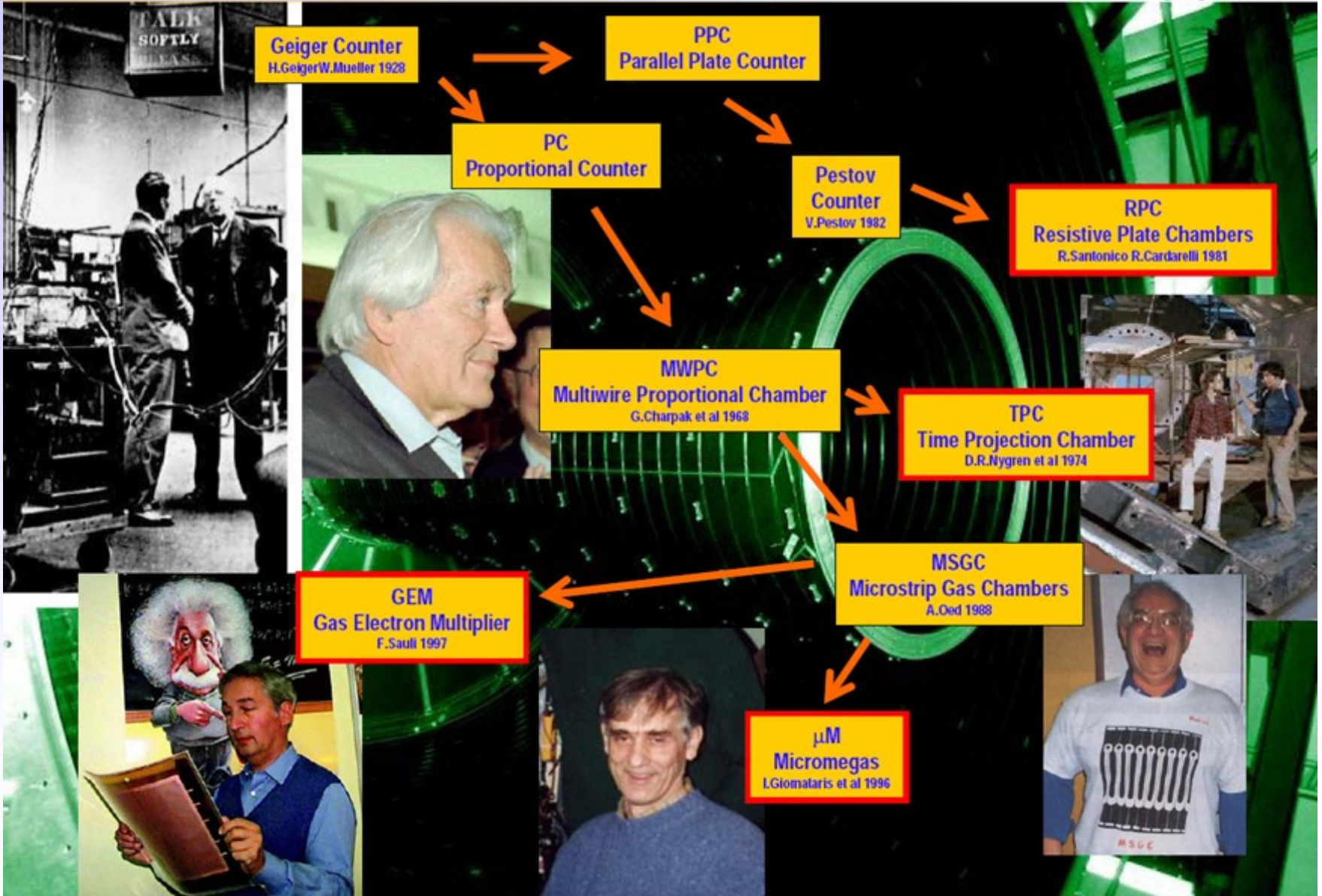
NA61



Totem Upgrade

□ Gaseous Detectors

- Ionization of Gases
- Gas Amplification
- Single Wire Proportional Chamber
- Drift Chamber
- Drift and Diffusion of Charge Carriers in Gases
- Examples of Detectors (MWPC, CSC, RPC, TPC)
- New Technologies – Micropattern Detectors (MSGC, Micromegas, GEM)
- Limitations of Gas Detectors
- Gas Detectors Simulations
- Applications
- Production Aspects



“Classic” Particle Detectors

- The Geiger-Müller tube (1928 by Hans Geiger and Walther Müller)
 - Tube filled with inert gas (He, Ne, Ar) + organic vapour
 - Central thin wire (20 – 50 μm \varnothing) , high voltage (several 100 Volts) between wire and tube



E. Rutherford 1909

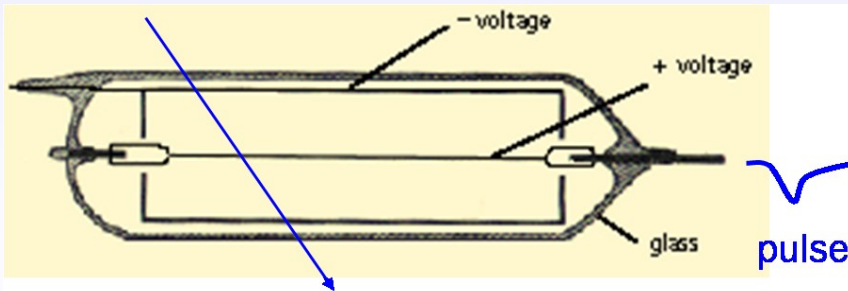


H. Geiger 1927

- Strong increase of E-field close to the wire
 - electron gains more and more energy
- above some threshold (>10 kV/cm)
 - electron energy high enough to ionize other gas molecules
 - newly created electrons also start ionizing
- **avalanche effect**: exponential increase of # electrons (and ions)

measurable signal on wire

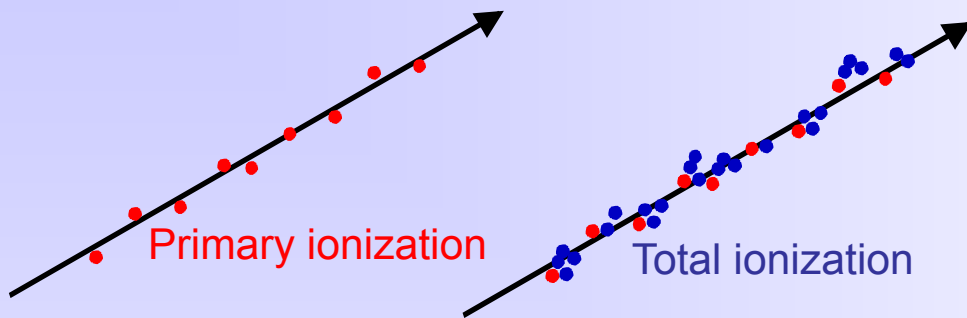
organic substances responsible for “quenching” (stopping) the discharge



First electrical signal from a particle

E. Rutherford and H. Geiger, Proc. Royall Soc. A81 (1908) 141

H. Geiger and W. Müller, Phys. Zeits. 29 (1928) 839



Lohse and Witzeling, Instrumentation In High Energy Physics, World Scientific, 1992

Fast charged particles ionize atoms of gas.
Often resulting primary electron will have enough kinetic energy to ionize other atoms.

$$n_{total} = \frac{\Delta E}{W_i} = \frac{dE}{dx} \frac{\Delta x}{W_i}$$

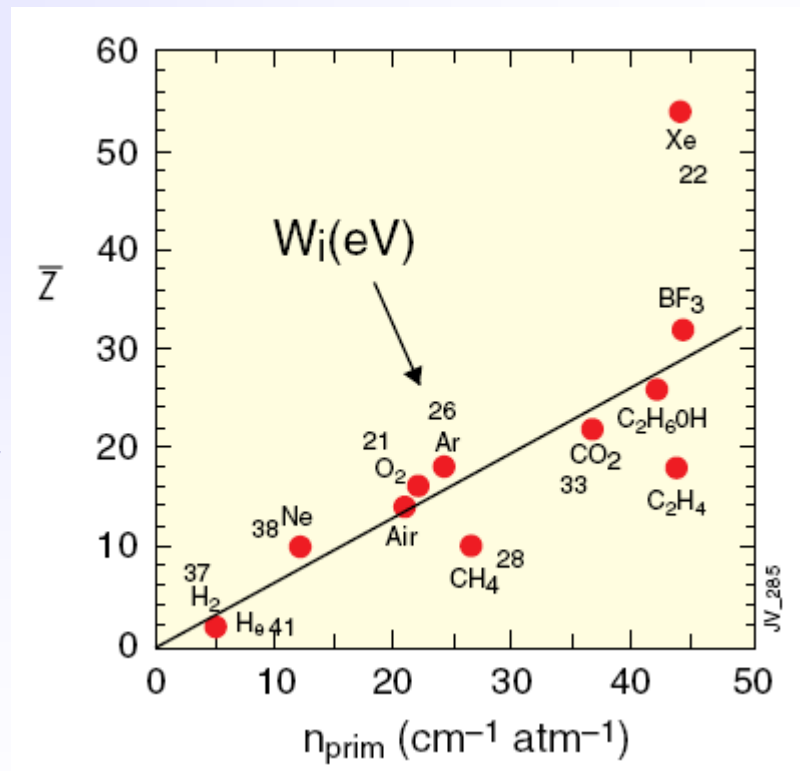
n_{total} - number of created electron-ion pairs

ΔE = total energy loss

W_i = effective <energy loss>/pair

$$n_{total} \approx 3 \dots 4 \cdot n_{primary}$$

Number of primary electron/ion pairs in frequently used gases.



- The actual number of **primary** electron/ion pairs is **Poisson** distributed.

$$P(m) = \frac{\bar{n}^m e^{-\bar{n}}}{m!} \quad \bar{n} = \frac{L}{\lambda} = LN\sigma_i$$

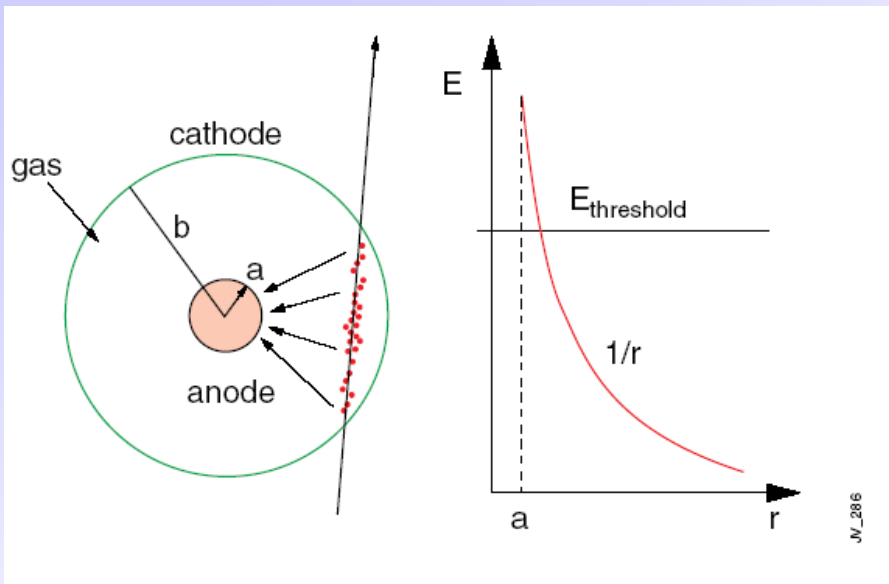
The detection efficiency is therefore limited to :

$$\varepsilon_{\text{det}} = 1 - P(0) = 1 - e^{-\bar{n}}$$

For thin layers ε_{det} can be significantly lower than 1.

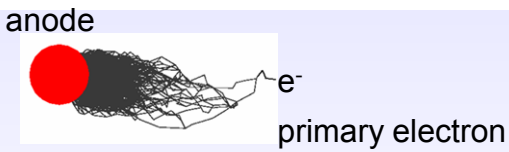
For example for 1 mm layer of Ar $n_{\text{primary}} = 2.5 \rightarrow \varepsilon_{\text{det}} = 0.92$.

- 100 electron/ion pairs created during ionization process is not easy to detect.
Typical noise of the amplifier $\approx 1000 e^-$ (ENC) \rightarrow gas amplification .



Electrons liberated by ionization drift towards the anode wire.

Electrical field close to the wire (typical wire \varnothing ~few tens of μm) is sufficiently high for electrons (above 10 kV/cm) to gain enough energy to ionize further \rightarrow **avalanche** – exponential increase of number of electron ion pairs.

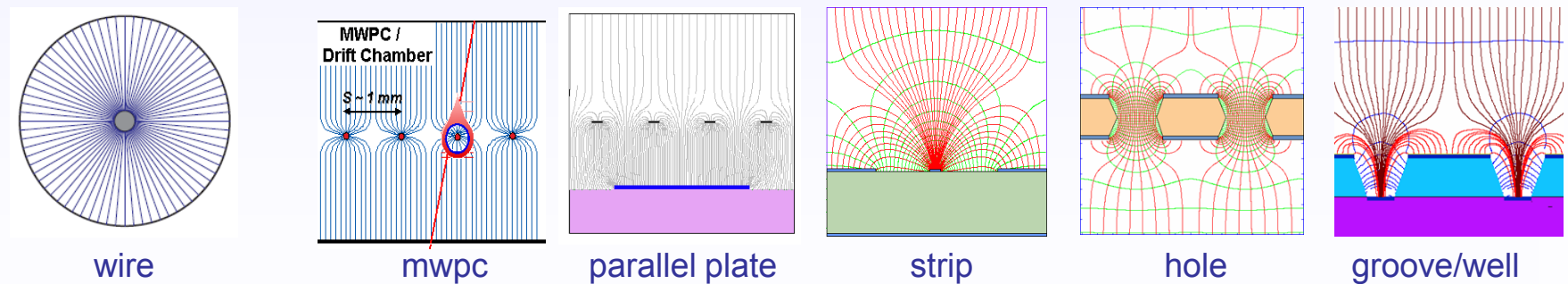


$$E(r) = \frac{CV_0}{2\pi\epsilon_0} \cdot \frac{1}{r}$$

C – capacitance/unit length

$$V(r) = \frac{CV_0}{2\pi\epsilon_0} \cdot \ln \frac{r}{a}$$

Cylindrical geometry is not the only one able to generate strong electric field:



Multiplication of ionization is described by the first Townsend coefficient $\alpha(E)$

$$dn = n\alpha dx \quad \alpha = \frac{1}{\lambda} \quad \lambda - \text{mean free path}$$

$$n = n_0 e^{\alpha(E)x} \quad \text{or} \quad n = n_0 e^{\alpha(r)x}$$

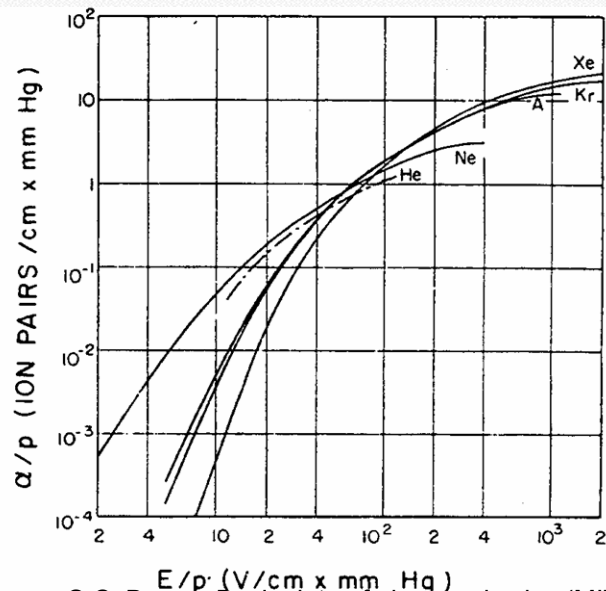
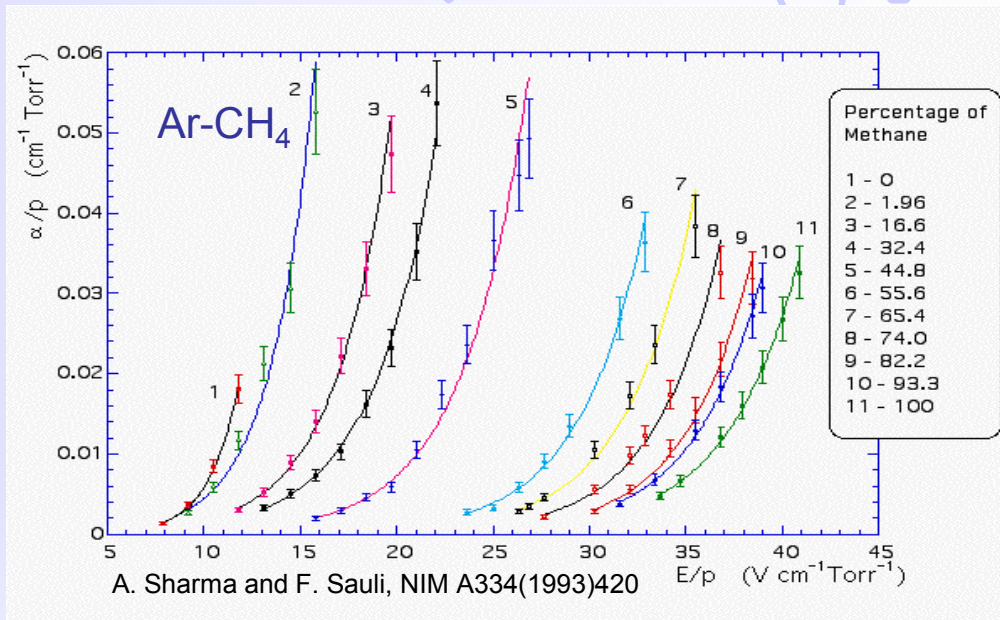
$\alpha(E)$ is determined by the excitation and ionization cross sections of the electrons in the gas.

It depends also on various and complex energy transfer mechanisms between gas molecules.

There is no fundamental expression for $\alpha(E)$ → it has to be measured for every gas mixture.

$$M = \frac{n}{n_0} = \exp \left[\int_a^{r_c} \alpha(r) dr \right]$$

Amplification factor or
Gain

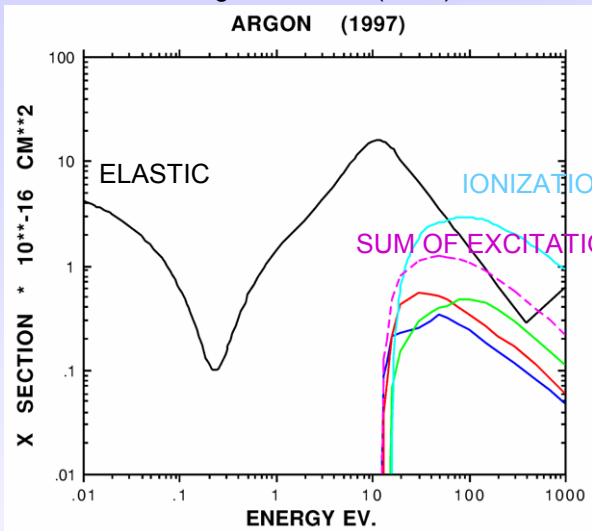


S.C. Brown, Basic data of plasma physics (MIT Press, 1959)

In the avalanche process molecules of the gas can be brought to excited states.

Solution: addition of polyatomic gas as a **quencher**

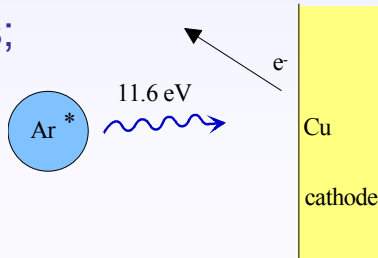
S. Biagi, NIM A421 (1999) 234



Absorption of photons in a large energy range (many vibrational and rotational energy levels).

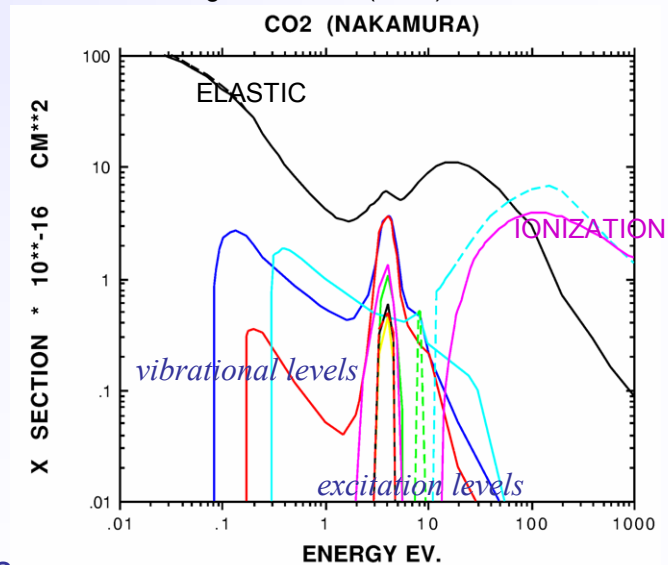
Energy dissipation by collisions or dissociation into smaller molecules.

De-excitation of noble gases only via emission of photons; e.g. 11.6 eV for Ar. This is above ionization threshold of metals; e.g. Cu 7.7 eV.



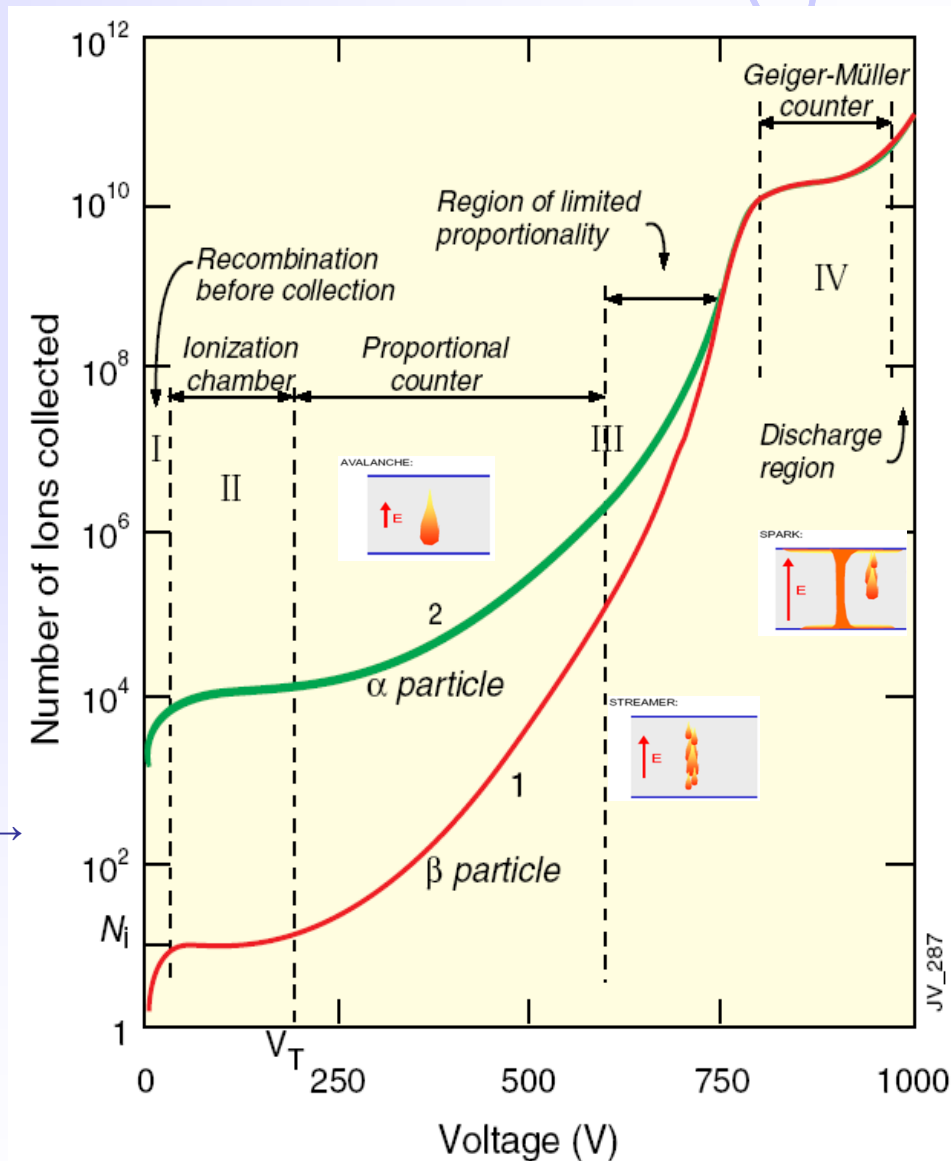
new avalanches → permanent discharges

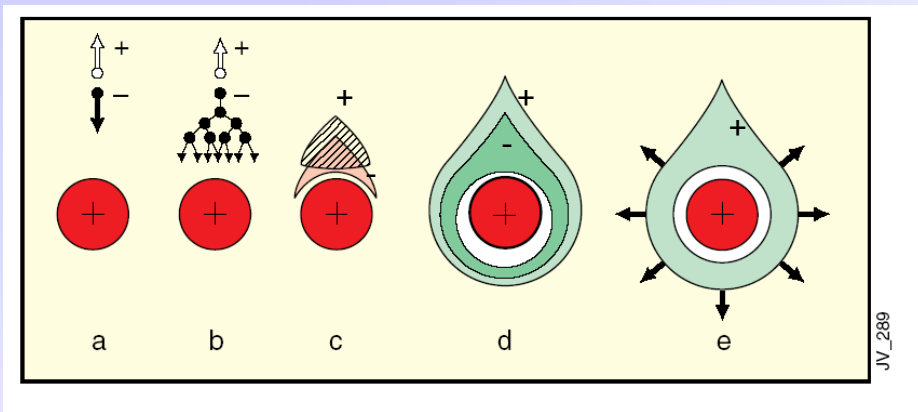
S. Biagi, NIM A421 (1999) 234



High Voltage

- I. **no collection** – ions recombine before collection
- II. **ionization mode** – full charge collection, but no charge multiplication; gain ~ 1
- III. **proportional mode** – multiplication of ionization starts; detected signal proportional to original ionization \rightarrow possible energy measurement (dE/dx); secondary avalanches have to be quenched; gain $\sim 10^4 - 10^5$
limited proportional mode (saturated, streamer) – strong photoemission; secondary avalanches merging with original avalanche; requires strong quenchers or pulsed HV; large signals \rightarrow simple electronics; gain $\sim 10^{10}$
- IV. **Geiger mode** – massive photoemission; full length of the anode wire affected; discharge stopped by HV cut; strong quenchers needed as well



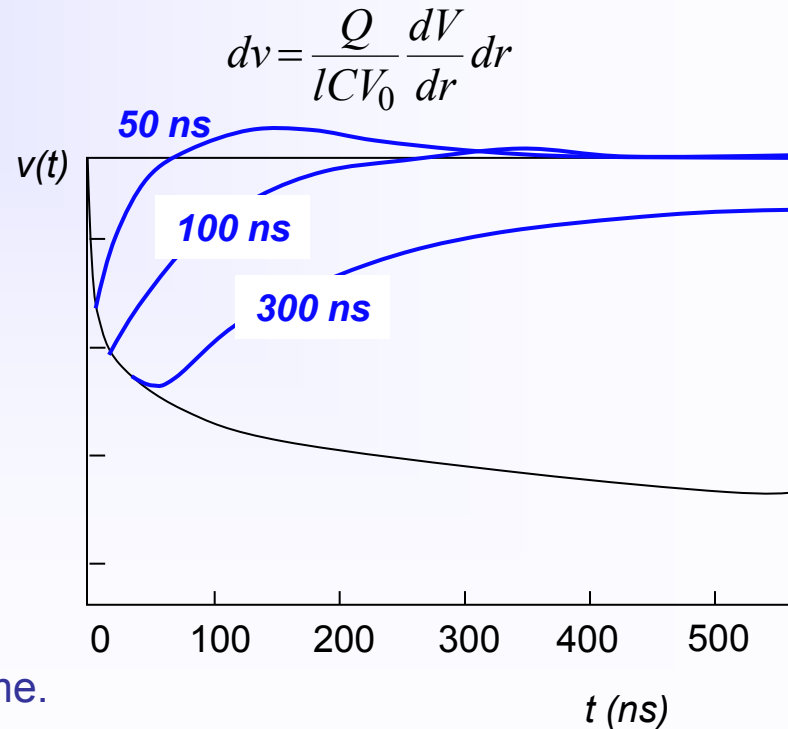


Electrons collected by the anode wire i.e. dr is very small (few μm). Electrons contribute only very little to detected signal (few %).

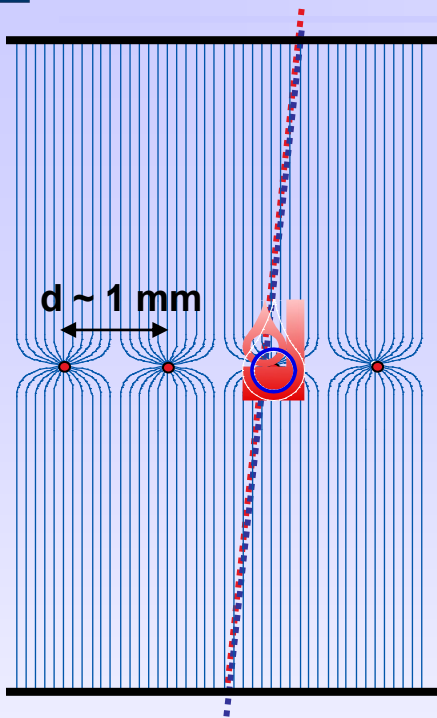
Ions have to drift back to cathode i.e. dr is large (few mm). Signal duration limited by total ion drift time.

Need electronic signal differentiation to limit dead time.

Avalanche formation within a few wire radii and within $t < 1$ ns.
Signal induction both on anode and cathode due to moving charges (both electrons and ions).



Multiwire Proportional Chamber



- Simple idea to multiply SWPC cell : Nobel Prize 1992
- First electronic device allowing high statistics experiments !!



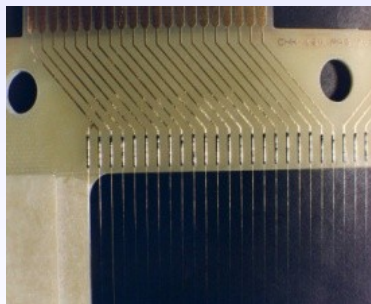
Georges Charpak

Typical geometry
5mm, 1mm, 20 μm

Normally digital readout :
spatial resolution limited to

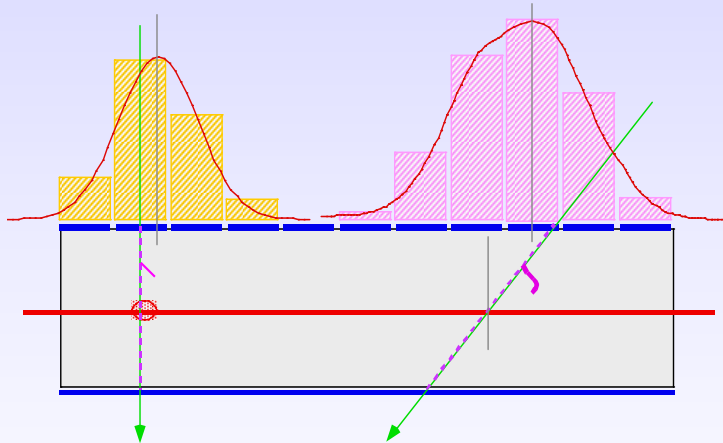
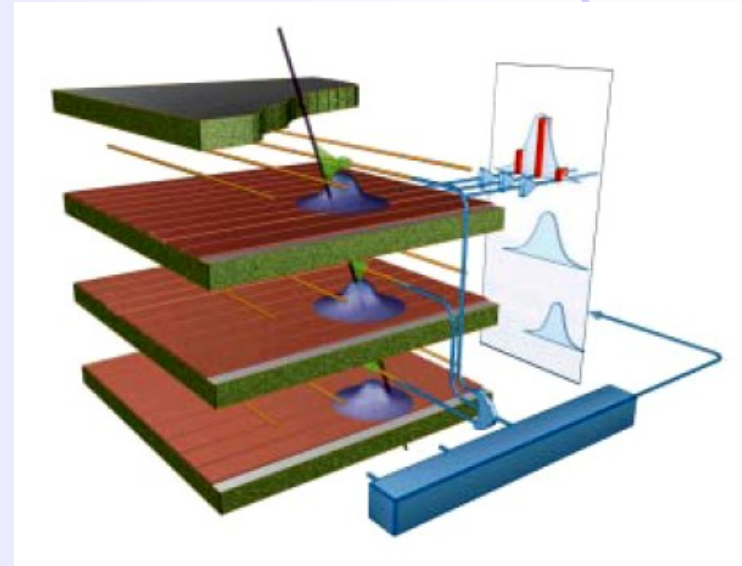
$$\sigma_x \approx \frac{d}{\sqrt{12}}$$

for $d = 1 \text{ mm}$ $\sigma_x = 300 \mu\text{m}$

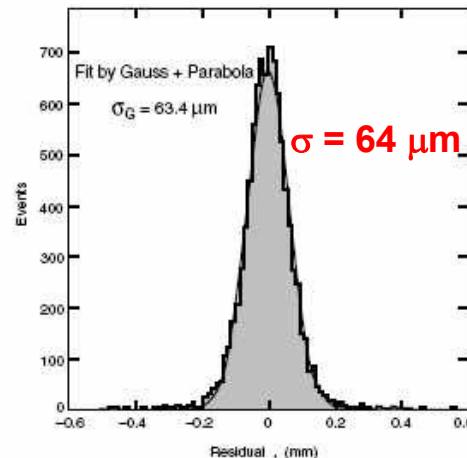


G. Charpak, F. Sauli and J.C. Santiard

Precise measurement of the second coordinate by interpolation of the signal induced on pads.
 Closely spaced wires makes CSC fast detector.



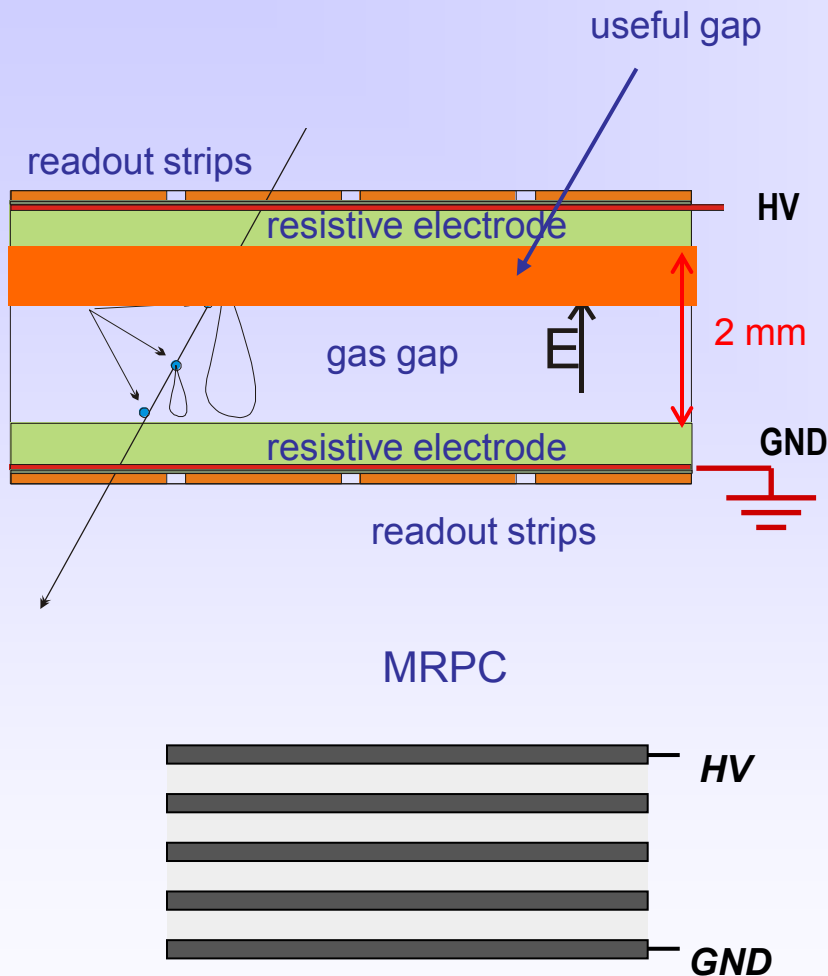
Center of gravity of induced signal method.



Space resolution



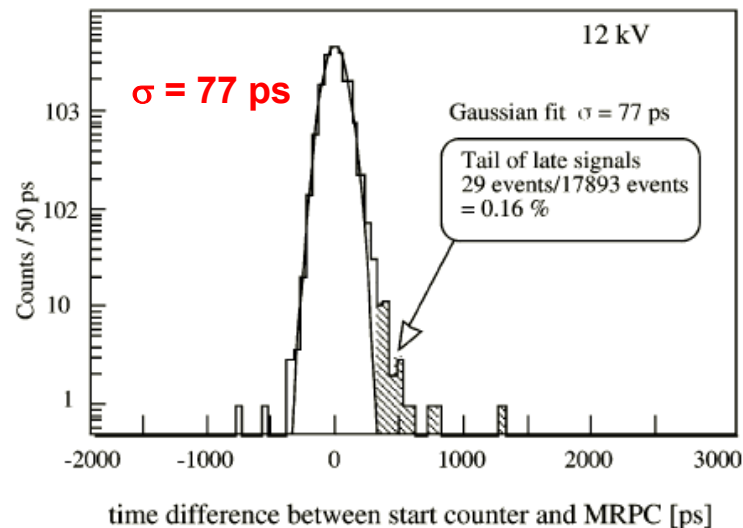
CMS



Rate capability strong function of the resistivity of electrodes in streamer mode.

A. Akindinov et al., NIM A456(2000)16

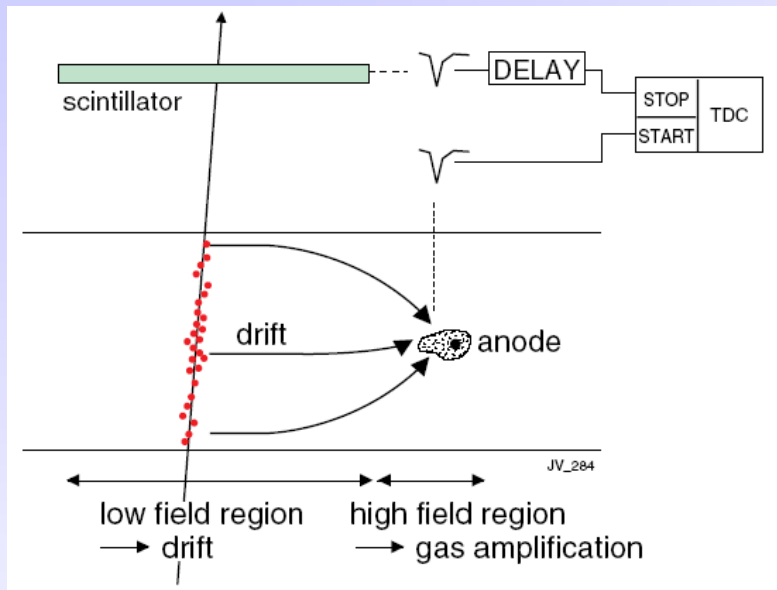
Typical time spectrum from 5 gap MRPC



Time resolution

Multigap RPC - exceptional time resolution suited for the trigger applications

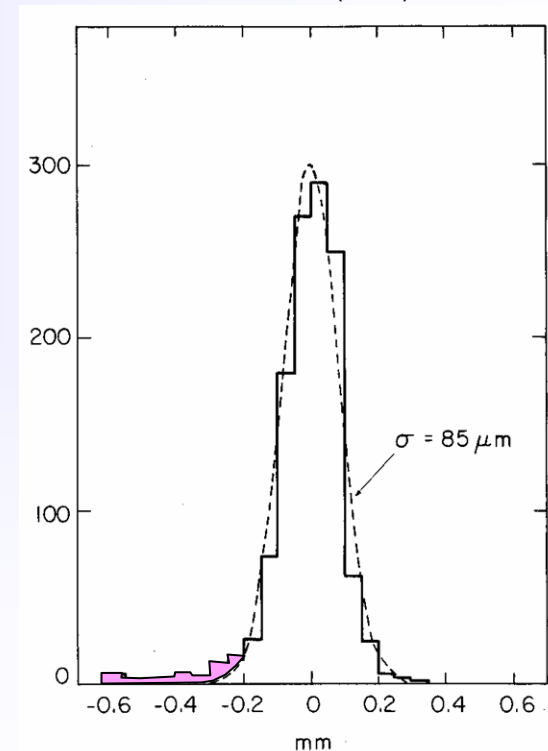
Spatial information obtained by measuring time of drift of electrons



Measure arrival time of electrons at sense wire relative to a time t_0 .
 Need a trigger (bunch crossing or scintillator).
 Drift velocity independent from E .

$$s = \int_{t_{start}}^{t_{stop}} v_D dt$$

F. Sauli, NIM 156(1978)147

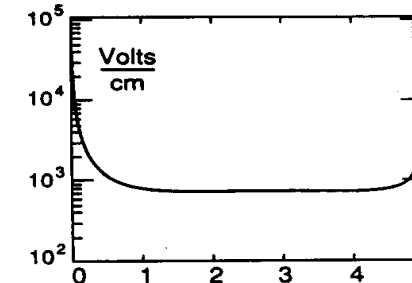
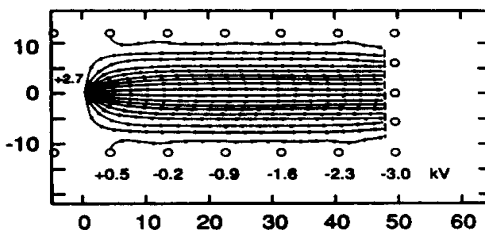
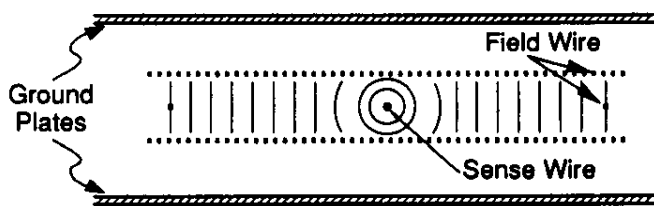
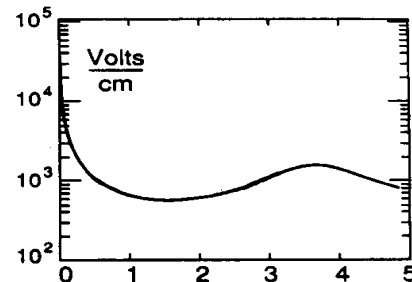
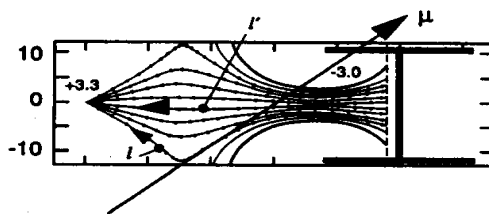
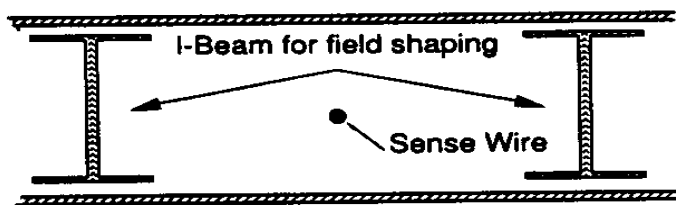
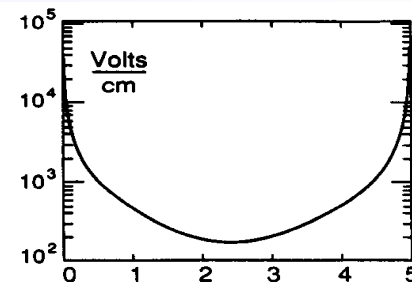
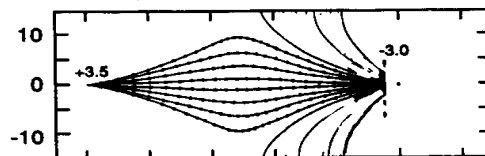
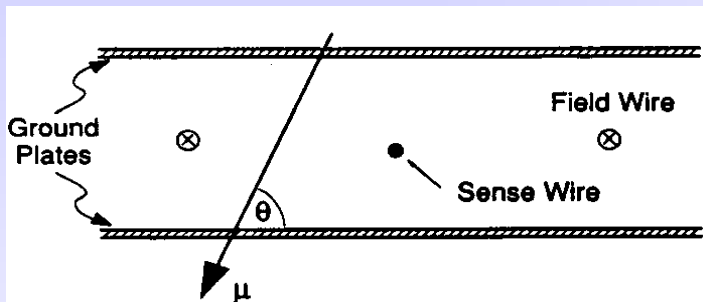


Advantages: smaller number of electronics channels.

Resolution determined by diffusion, primary ionization statistics, path fluctuations and electronics.

Planar drift chamber designs

Essential: linear space-time relation; constant E-field; little dependence of v_D on E.

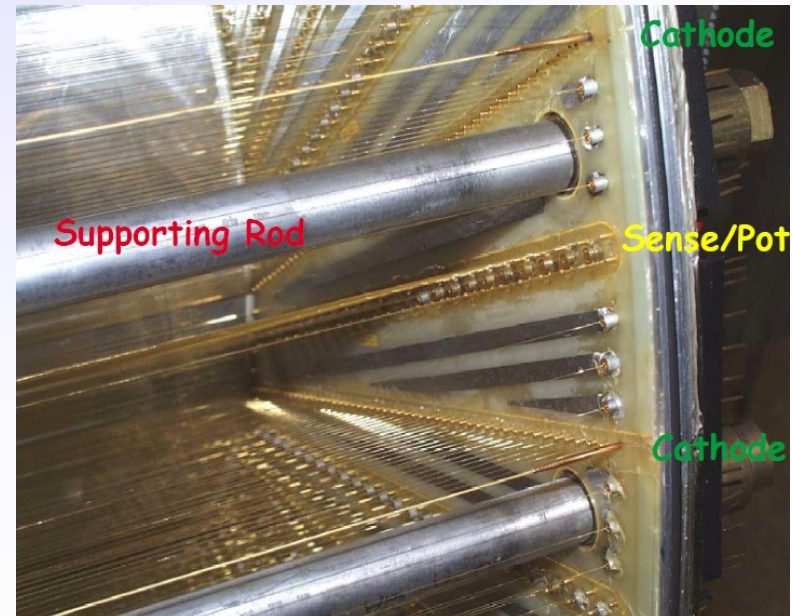
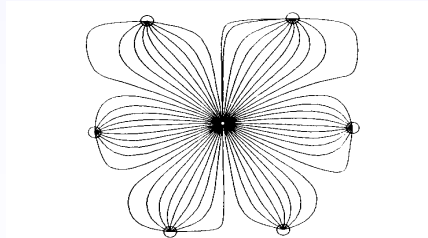
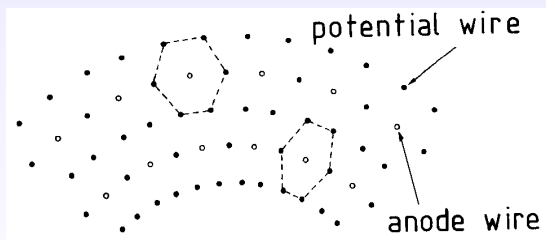
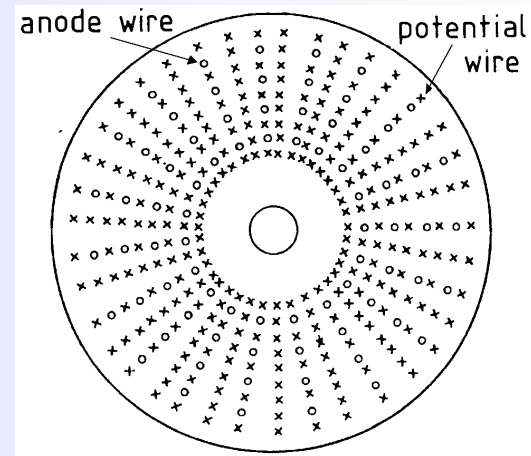
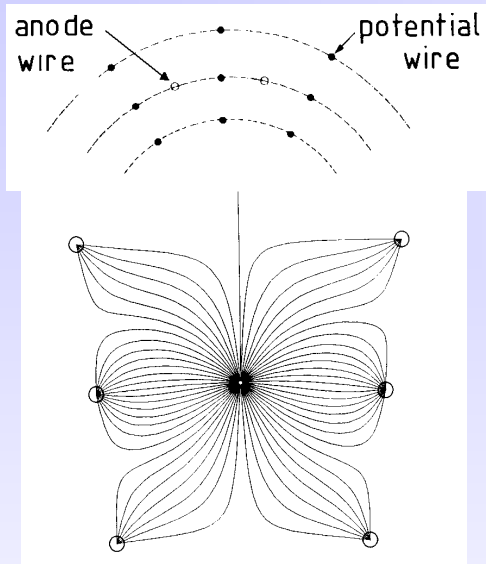


[mm]

[cm]

U. Becker in Instrumentation in High Energy Physics, World Scientific

Various geometries of cylindrical drift chambers



Free ionization charges lose energy in collisions with gas atoms and molecules (thermalization).

Maxwell - Boltzmann energy distribution:

$$F(\epsilon) = \text{const} \sqrt{\epsilon} e^{-\frac{\epsilon}{kT}}$$

Average (thermal) energy:

$$\epsilon_T = \frac{3}{2} kT \approx 0.040 \text{ eV}$$

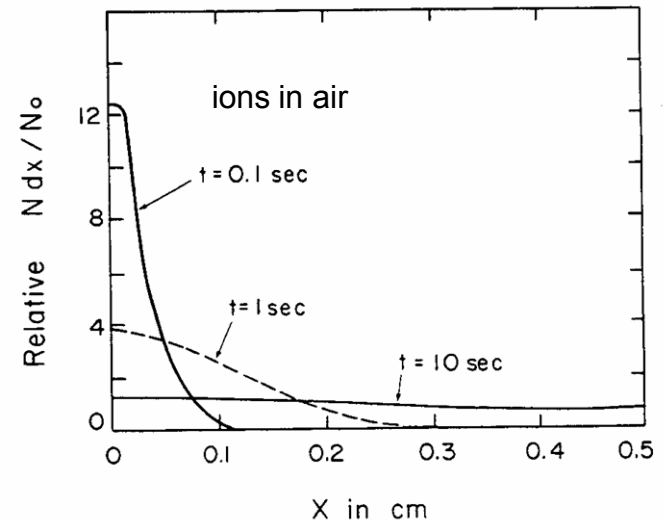
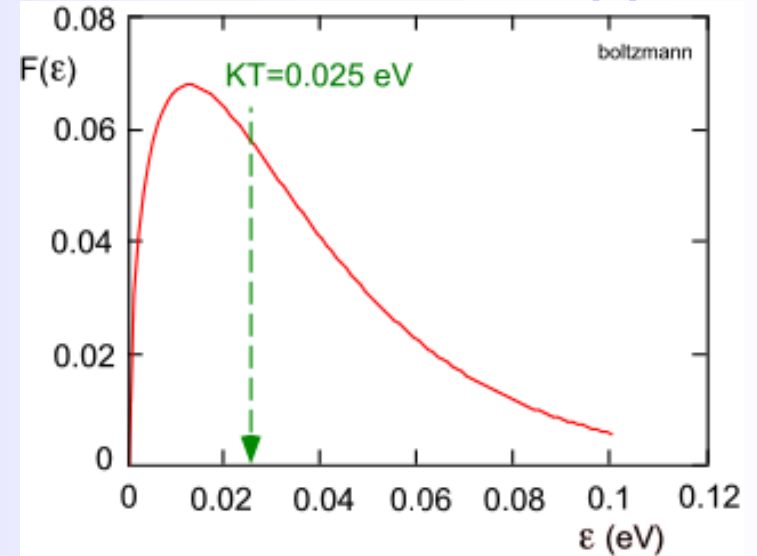
Diffusion equation:

Fraction of free charges at distance x after time t .

$$\frac{dN}{N} = \frac{1}{\sqrt{4\pi Dt}} e^{-\frac{x^2}{4Dt}} dt \quad D: \text{diffusion coefficient}$$

RMS of linear diffusion:

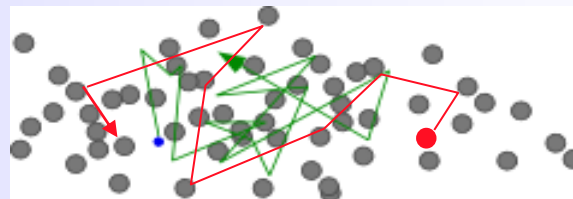
$$\sigma_x = \sqrt{2Dt}$$



L.B. Loeb, Basic processes of gaseous electronics
Univ. of California Press, Berkeley, 1961

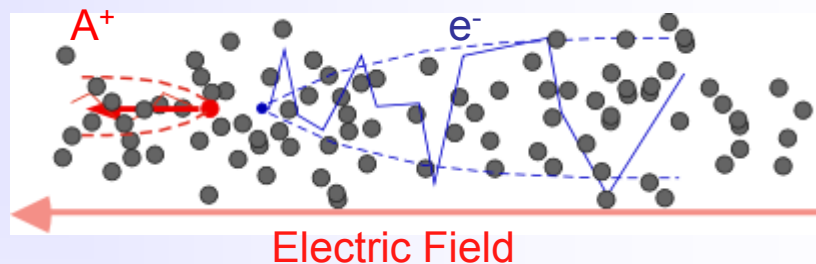
$E=0$ thermal diffusion

$$\langle v \rangle_t = 0$$



$E>0$ charge transport and diffusion

$$\langle v \rangle_t = v_D$$



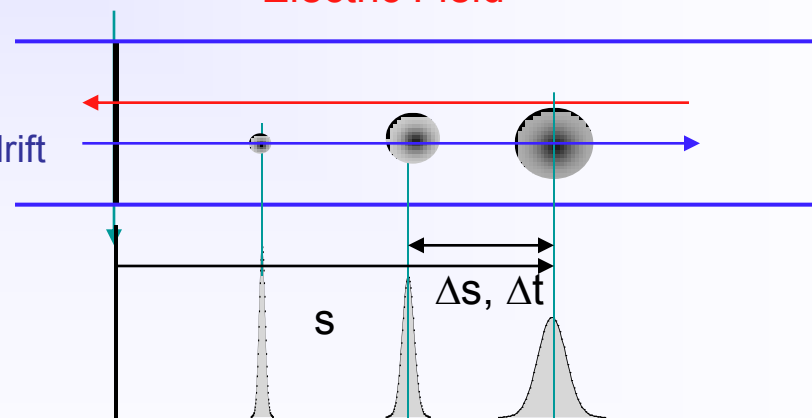
$$v_D = \frac{\Delta s}{\Delta t}$$

$$\sigma_x = \sqrt{2Dt} = \sqrt{2D \frac{s}{v_D}}$$

Electron swarm drift

Drift velocity

Diffusion



Drift velocity of ions

is almost linear function of E $v_D^{ion} = \mu^{ion} E$

Mobility: $\mu^{ion} = \frac{e\tau}{m}$ is

constant for given gas at fixed P and T,
direct consequence of the fact that
average energy of ion is unchanged
up to very high E fields.

Diffusion of ions

from microscopic picture can be shown:

$$\varepsilon = \frac{3De}{2\mu}$$

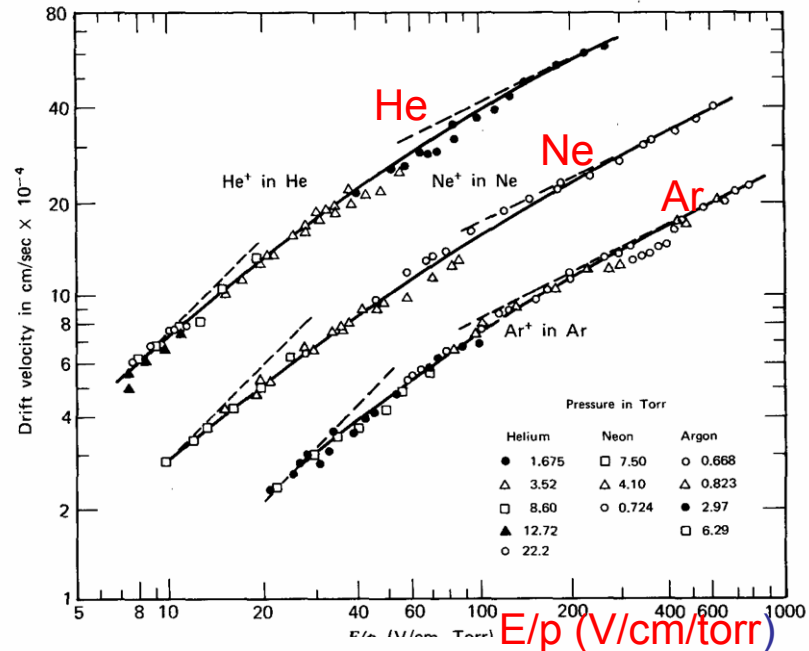
$$\frac{D}{\mu^{ion}} = \frac{kT}{e}$$

→

$$\sigma_x^{ion} = \sqrt{\frac{2kTx}{eE}}$$

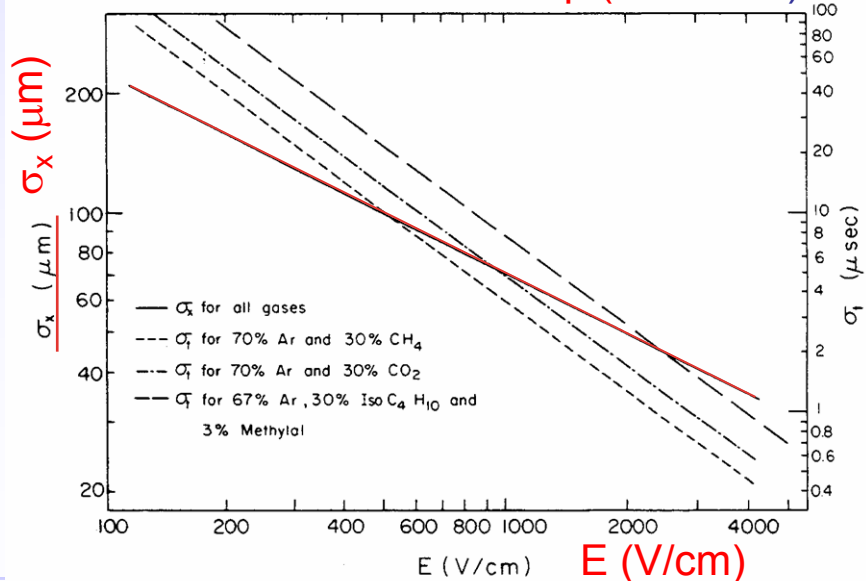
thermal limit

the same for all gases !!



Drift velocity of ions

E. McDaniel and E. Mason
The mobility and diffusion of ions in gases, Wiley 1973



$$v_D = \mu E = \frac{eE}{m} \tau$$

$$\frac{x}{v_D \tau} \lambda(\varepsilon) \varepsilon_E = eEx$$

Townsend expression; acceleration in the field times time between collisions

balance between energy acquired from the field and collision losses

$\frac{x}{v_D \tau}$ number of collisions; $\lambda(\varepsilon)$ fractional energy loss per collision

ε_E part of equilibrium energy not containing thermal motion

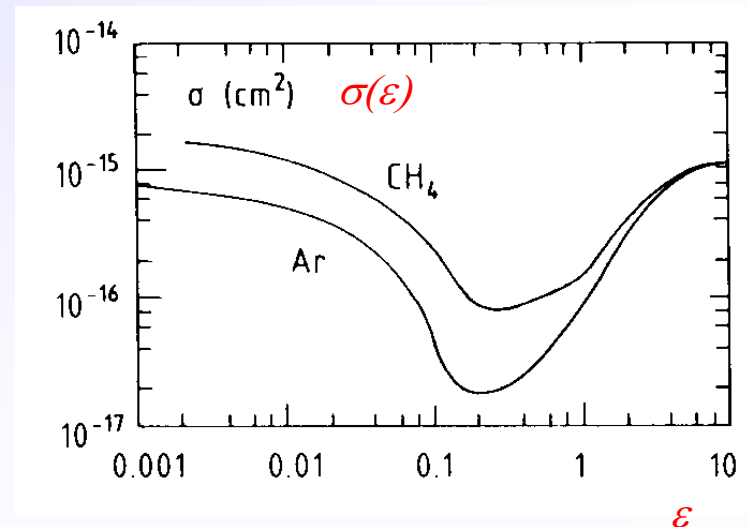
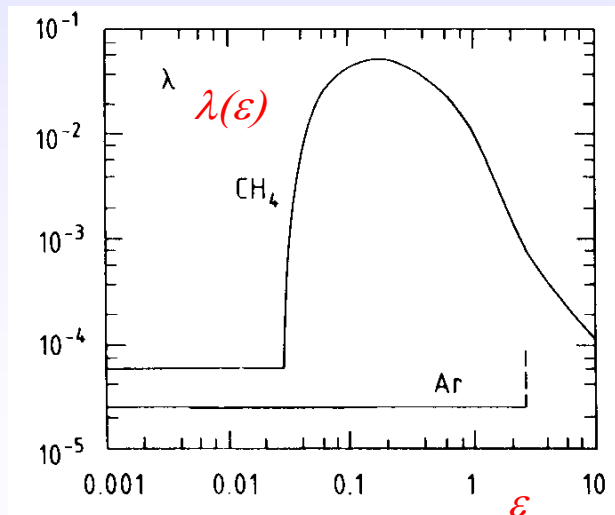
time between collisions; v instantaneous velocity

total energy

$$\tau = \frac{1}{N\sigma(\varepsilon)v}$$

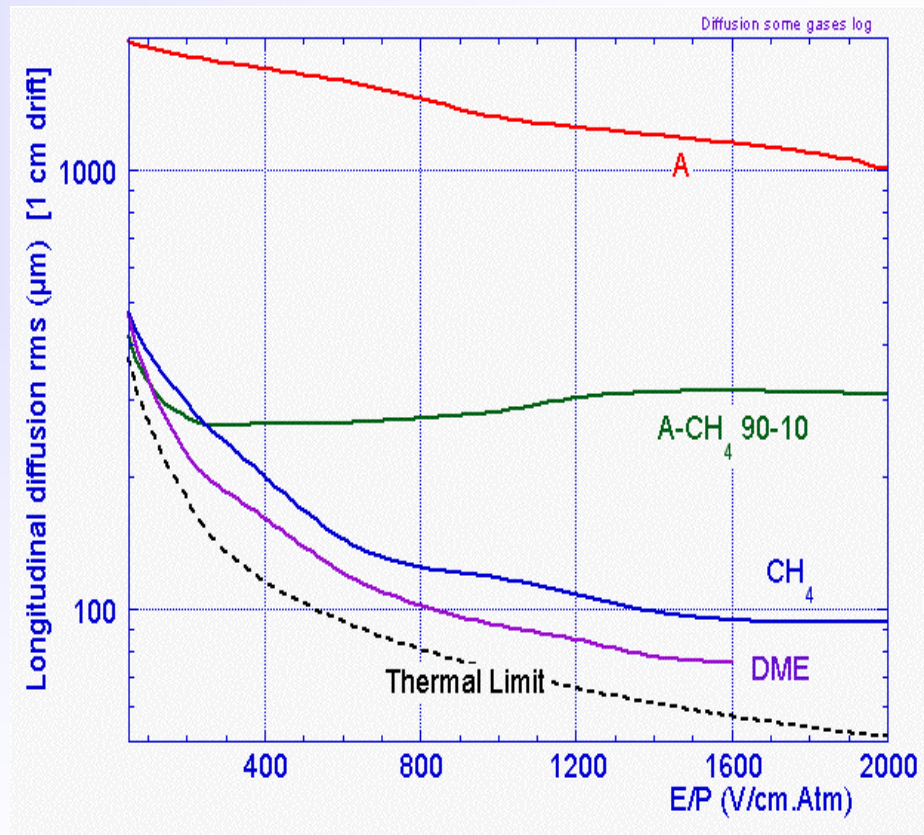
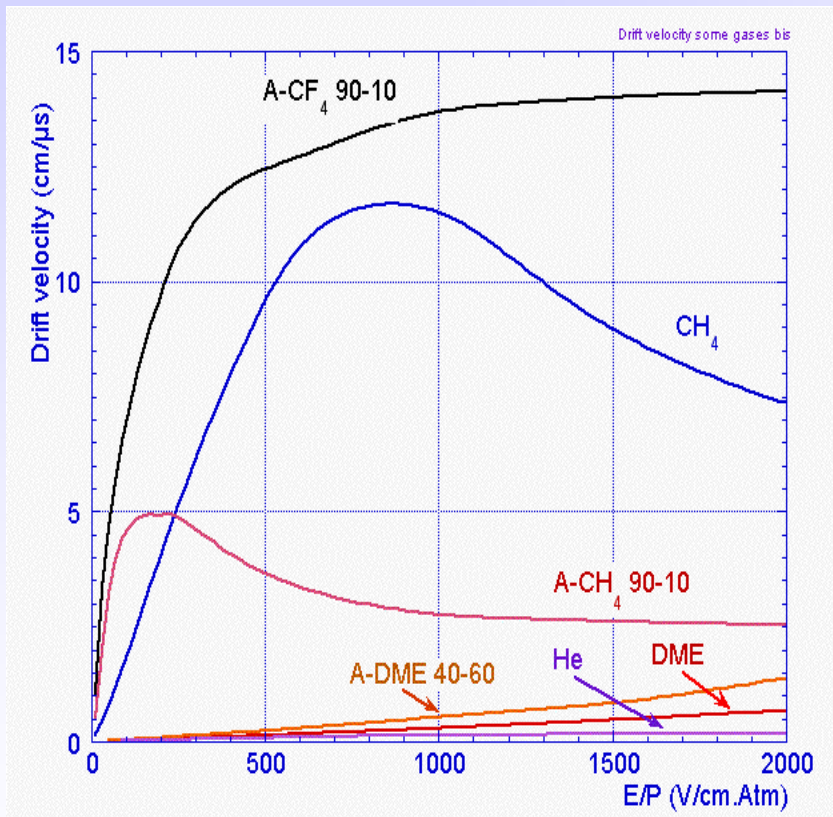
$$\varepsilon_E + \frac{3}{2}kT$$

$$v_D^2 = \frac{eE}{mN\sigma(\varepsilon)} \sqrt{\frac{\lambda(\varepsilon)}{2}}$$



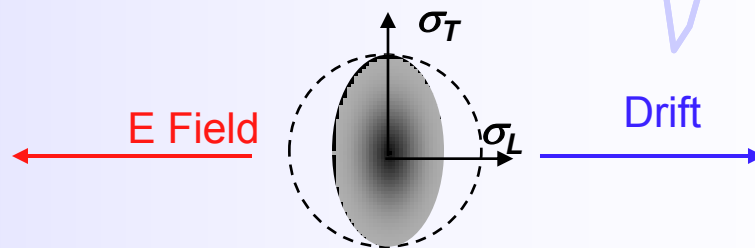
B. Schmidt, thesis, unpublished, 1986

Large range of drift velocity and diffusion:

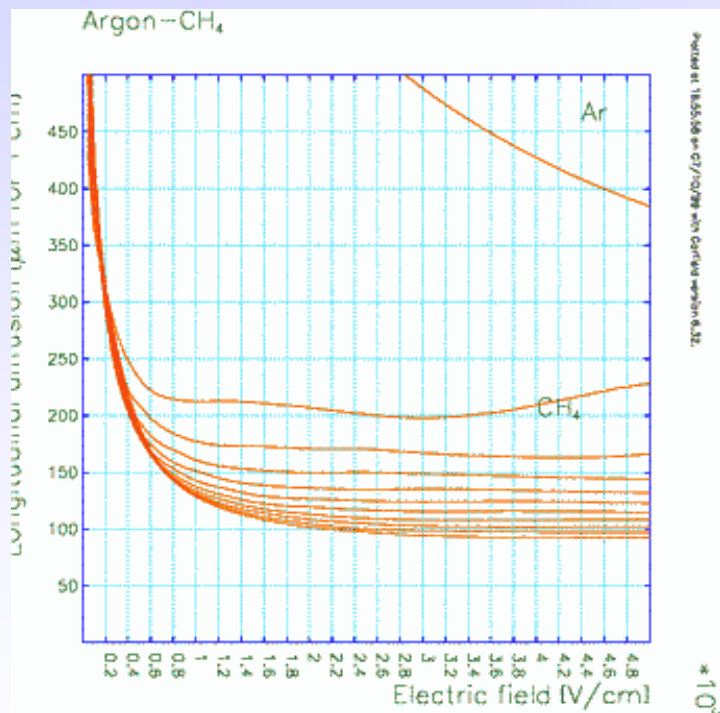


F. Sauli, IEEE Short Course on Radiation Detection and Measurement, Norfolk (Virginia) November 10-11, 2002

Influence of gas mixture composition on two diffusion coefficients

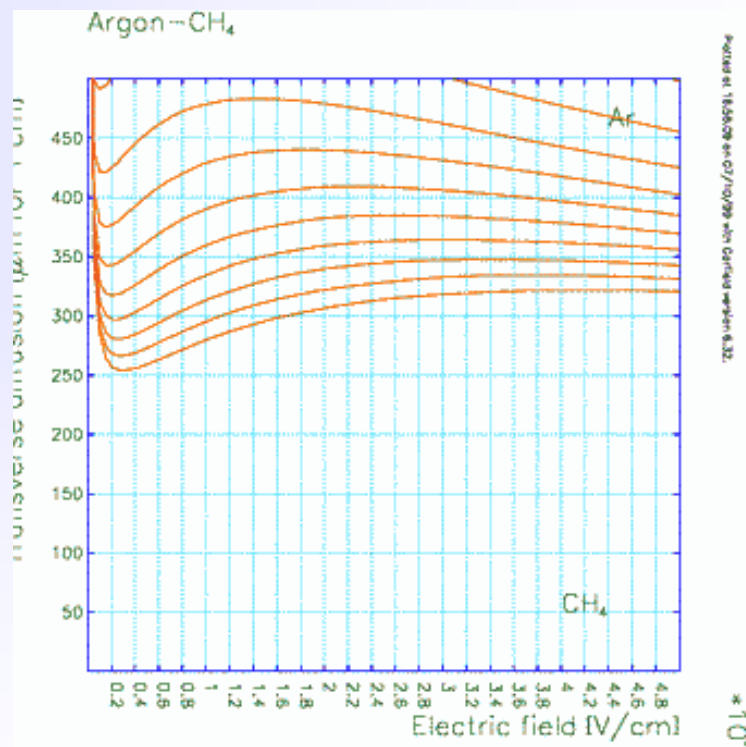


Longitudinal diffusion (μm for 1 cm drift)



E (V/cm)

Transverse diffusion (μm for 1 cm drift)



E(V/cm)

S. Biagi <http://consult.cern.ch/writeup/magboltz/>

Drift in Presence of E and B Fields

Equation of motion of free charge carriers in presence of E and B fields:

$$m \frac{d\vec{v}}{dt} = e\vec{E} + e(\vec{v} \times \vec{B}) + \vec{Q}(t) \quad \text{where } \vec{Q}(t) \text{ stochastic force resulting from collisions}$$

Time averaged solutions with assumptions: $\vec{v}_D = \langle \vec{v} \rangle = \text{const.}$; $\langle \vec{Q}(t) \rangle = \frac{m}{\tau} \vec{v}_D$ friction force

$$\left\langle \frac{d\vec{v}}{dt} \right\rangle = 0 = e\vec{E} + e(\vec{v}_D \times \vec{B}) - \frac{m}{\tau} \vec{v}_D \quad \tau \text{ mean time between collisions}$$

$$\vec{v}_D = \frac{\mu |\vec{E}|}{1 + \omega^2 \tau^2} \left[\hat{E} + \omega \tau (\hat{E} \times \hat{B}) + \omega^2 \tau^2 (\hat{E} \cdot \hat{B}) \hat{B} \right]$$

$$\mu = \frac{e\tau}{m} \text{ mobility} \quad \omega = \frac{eB}{m} \text{ cyclotron frequency}$$

$$B=0 \rightarrow \vec{v}_D^B = \vec{v}_D^0 = \mu \vec{E}$$

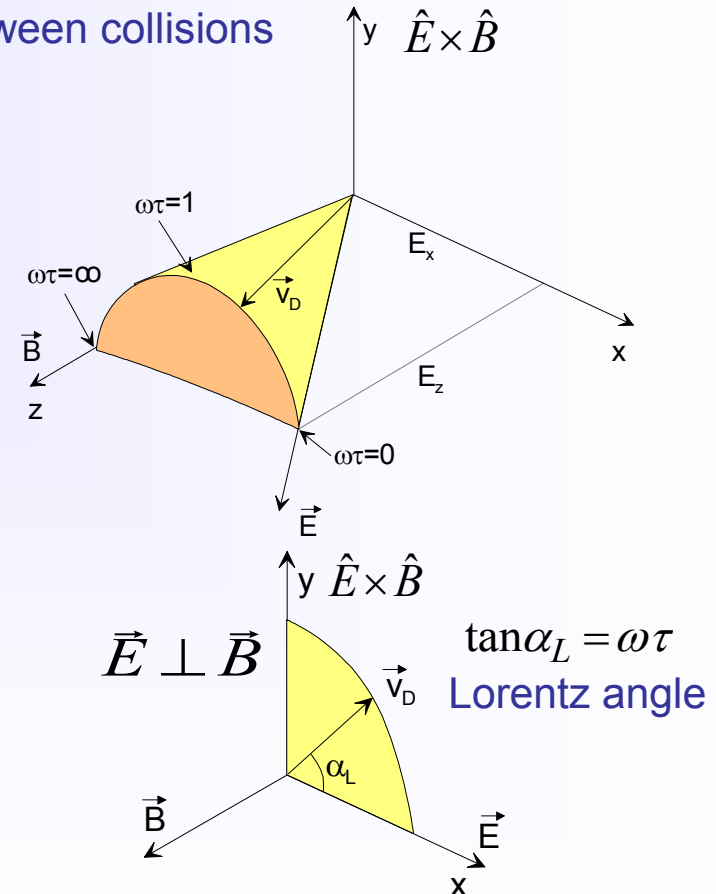
$$\vec{E} \parallel \vec{B} \rightarrow v_D^B = v_D^0$$

$$\vec{E} \perp \vec{B} \rightarrow v_D^B = \frac{E}{B} \frac{\omega \tau}{\sqrt{1 + \omega^2 \tau^2}}$$

In general drift velocity has 3 components: $\parallel \vec{E}; \parallel \vec{B}; \parallel \vec{E} \times \vec{B}$

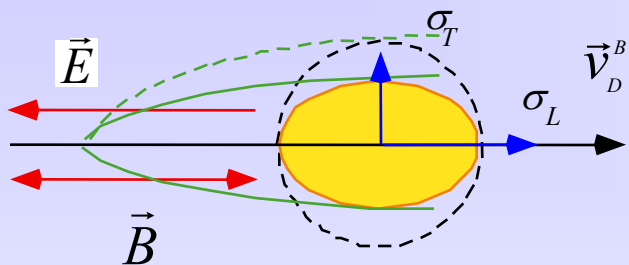
$\omega \tau \ll 1$ particles follow E-field

$\omega \tau \gg 1$ particles follow B-field



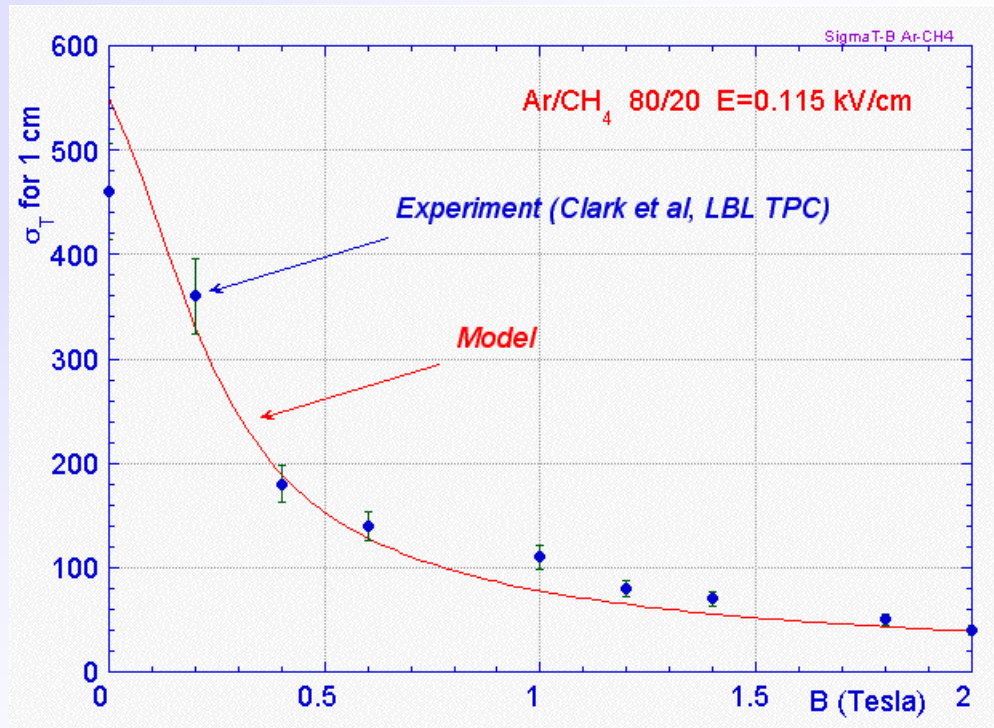
Diffusion Magnetic Anisotropy

$$\vec{E} \parallel \vec{B}$$

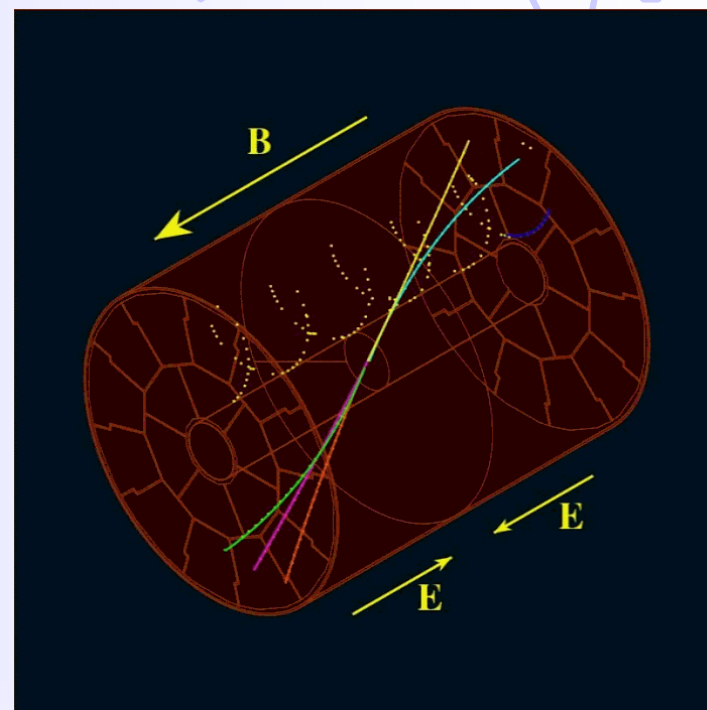
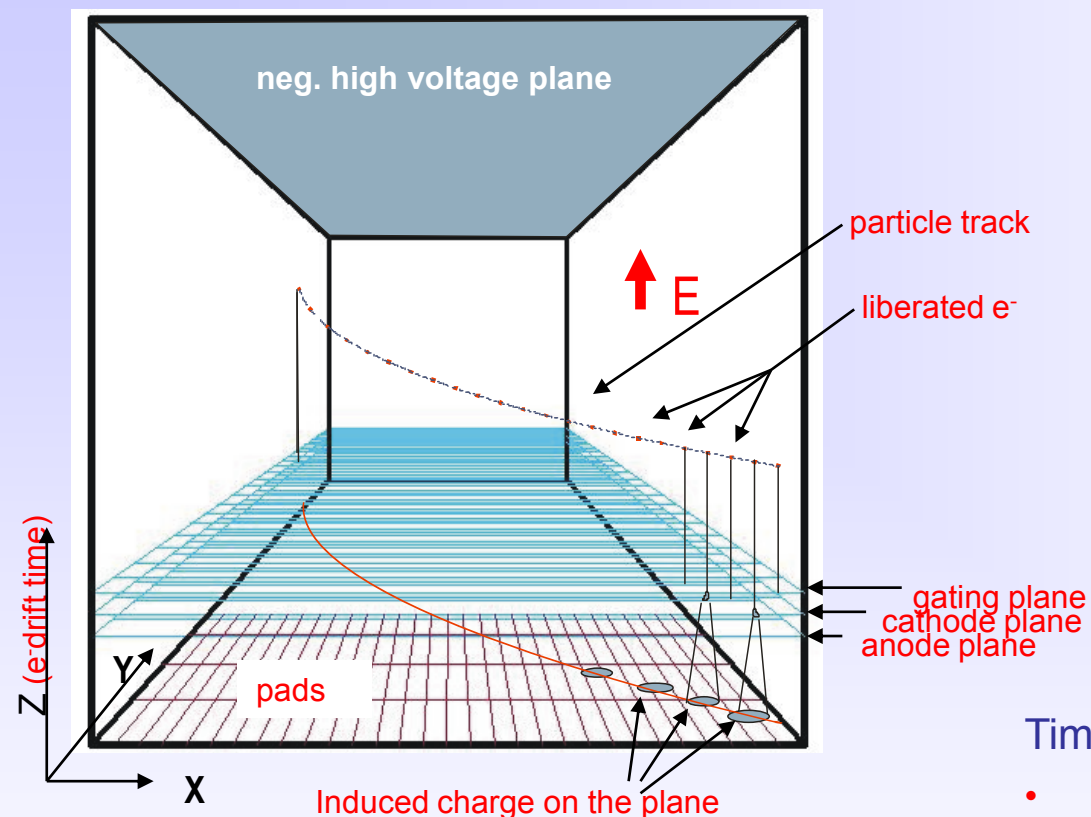


$$\sigma_L = \sigma_0$$

$$\sigma_T = \frac{\sigma_0}{\sqrt{1 + \omega^2 \tau^2}}$$

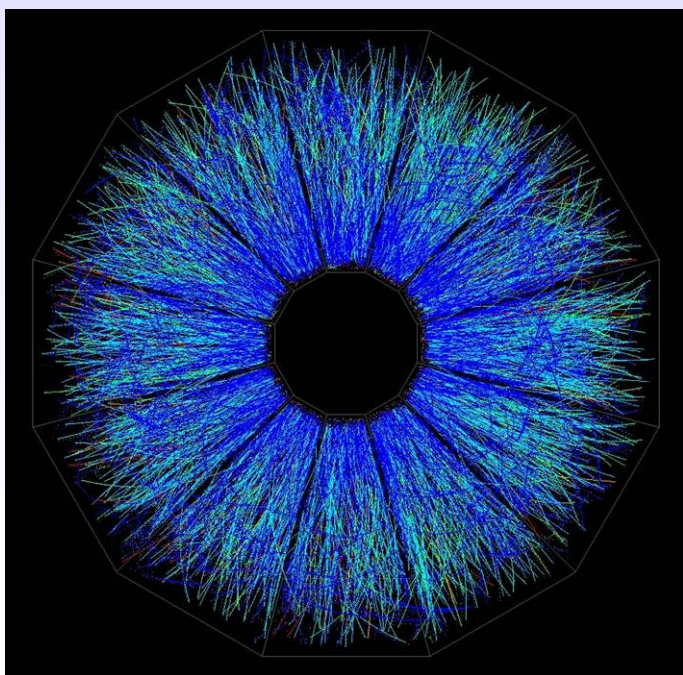
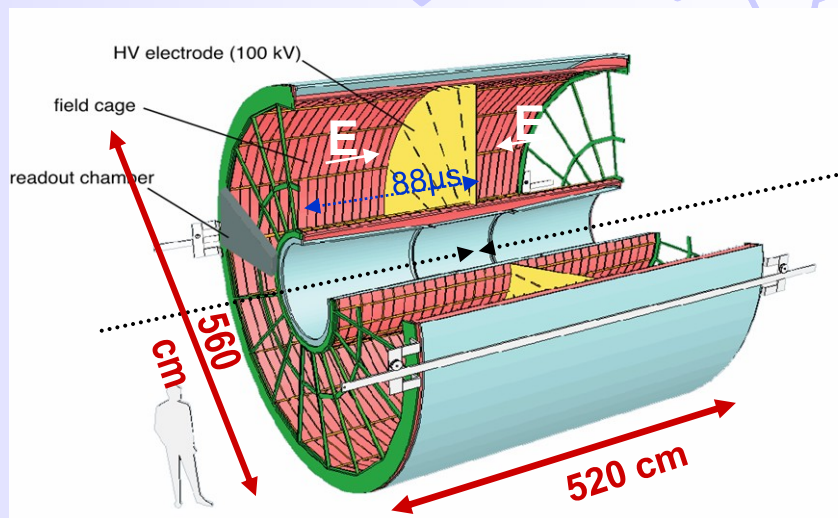
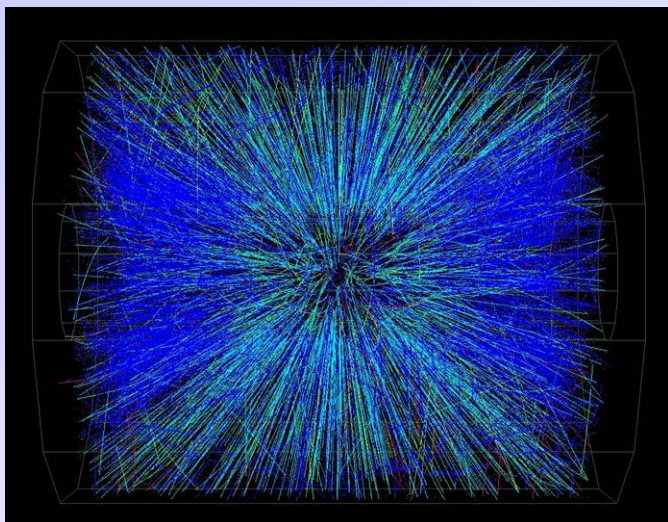


F. Sauli, IEEE Short Course on Radiation Detection and Measurement, Norfolk (Virginia) November 10-11, 2002



Time Projection Chamber

- full 3D track reconstruction: x - y from wires and segmented cathode of MWPC (or MPGD); $z = v_{\text{drift}} \times t_{\text{drift}}$ from drift time
- momentum resolution
space resolution + B field
(multiple scattering)
- energy resolution
measurement of primary ionization



Alice TPC

- HV central electrode at -100 kV
- Drift length 250 cm at $E=400$ V/cm
- Gas Ne-CO₂ 90-10
- Space point resolution ~ 500 μm
- dp/p 2% @ 1 GeV; 10% @ 10 GeV

Events from **STAR TPC** at RHIC

Au-Au collisions at CM energy of 130 GeV/n

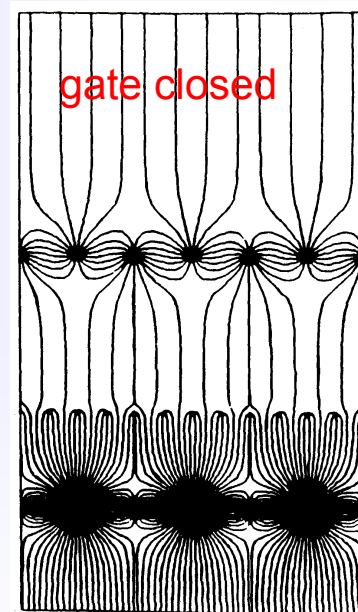
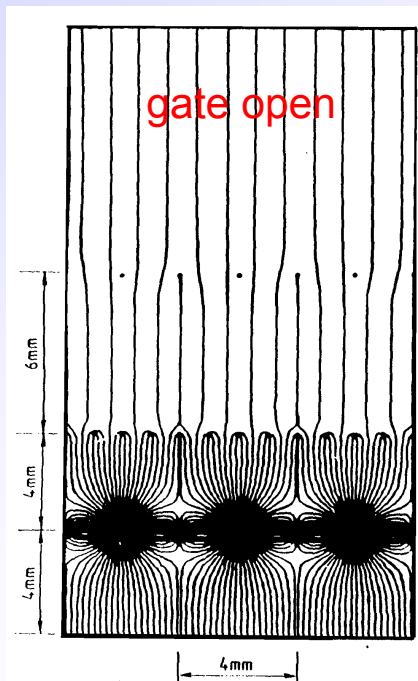
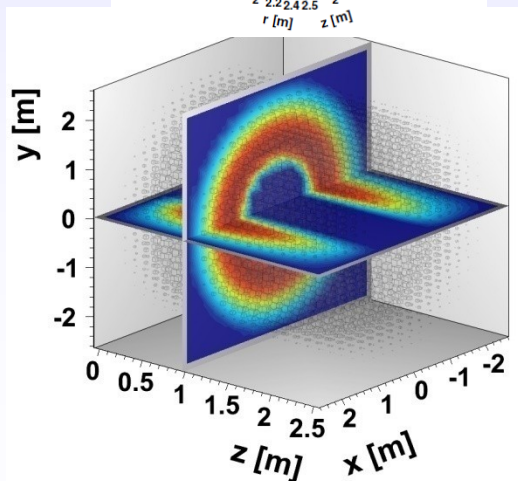
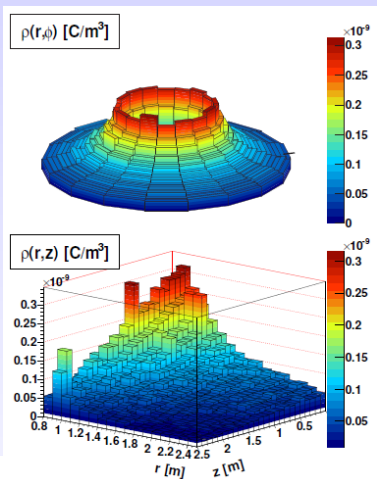
Typically ~ 2000 tracks/event

Positive ion backflow modifies electric field resulting in track distortion.

Solution : gating (or GEM)

Prevents electrons to enter amplification region in case of uninteresting event;

Prevents ions created in avalanches to flow back to drift region.



gating plane

cathode plane

anode wires

readout pads

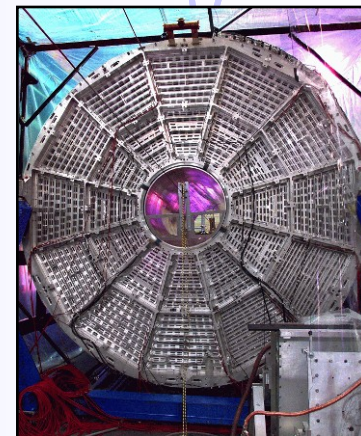
ALEPH coll., NIM A294(1990)121

PEP4 (SLAC)

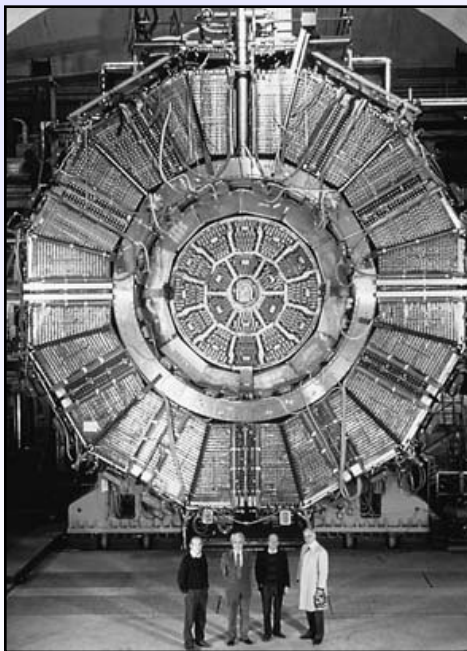


TPC	Reference
PEP4	PEP-PROPOSAL-004, Dec 1976
TOPAZ	Nucl. Instr. and Meth. A252 (1986) 423
ALEPH	Nucl. Instr. and Meth. A294 (1990) 121
DELPHI	Nucl. Instr. and Meth. A323 (1992) 209-212
NA49	Nucl. Instr. and Meth. A430 (1999) 210
STAR	IEEE Trans. on Nucl. Sci. Vol. 44, No. 3 (1997)

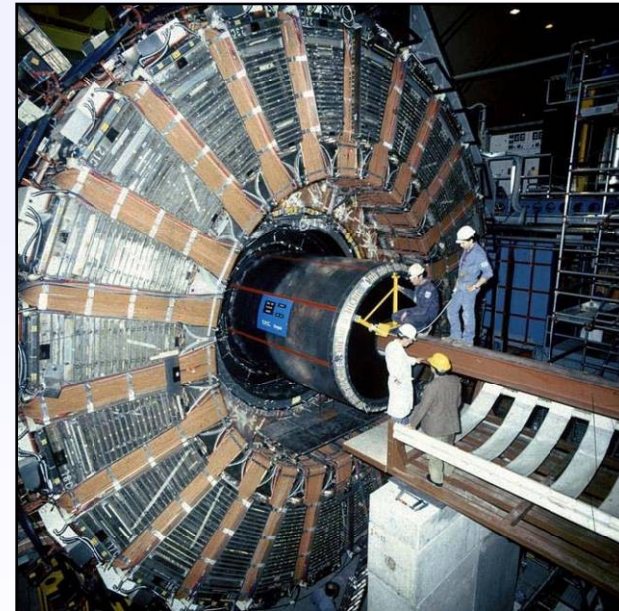
STAR (LBL)



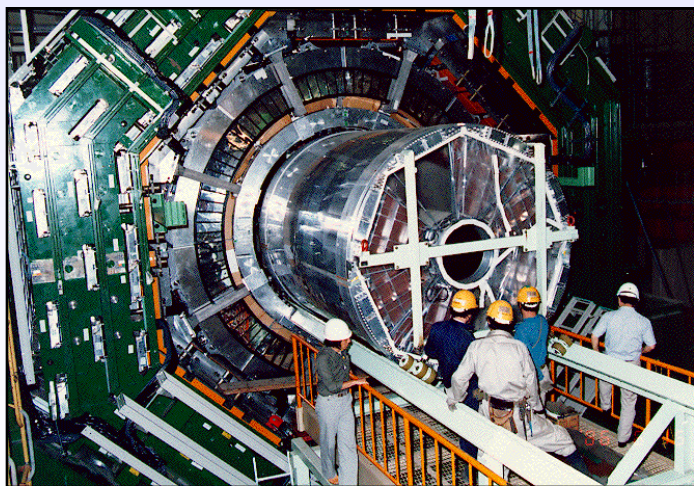
ALEPH (CERN)

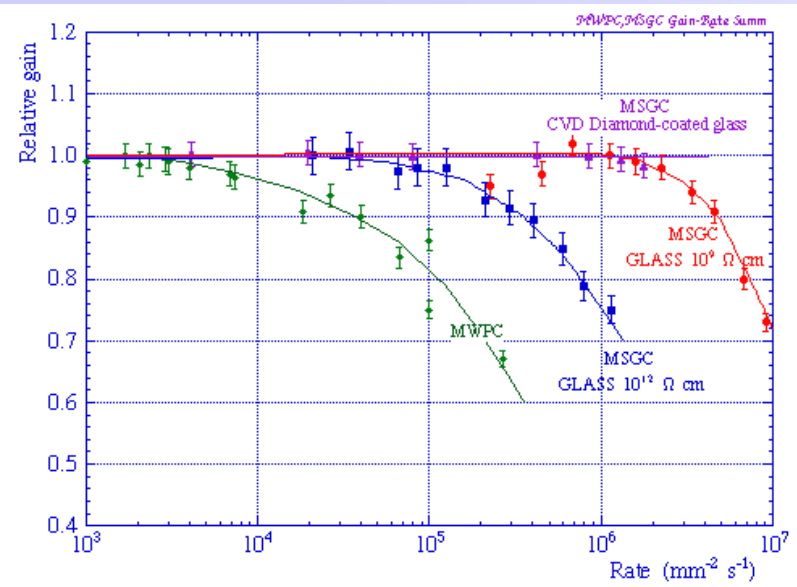


DELPHI (CERN)



TOPAZ (KEK)





Advantages of gas detectors:

- low radiation length
- large areas at low price
- flexible geometry
- spatial, energy resolution ...

Problem:

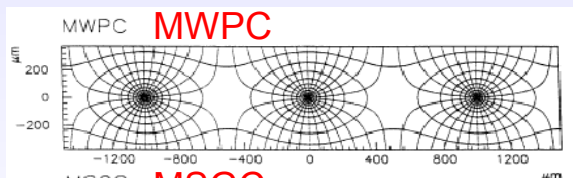
- rate capability limited by space charge defined by the time of evacuation of positive ions

Solution:

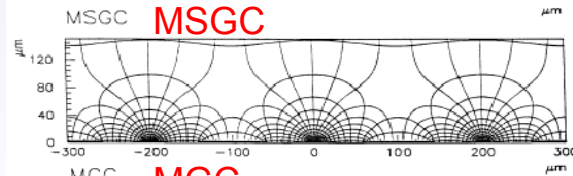
- reduction of the size of the detecting cell (limitation of the length of the ion path) using chemical etching techniques developed for microelectronics and keeping at same time similar field shape.

scale factor

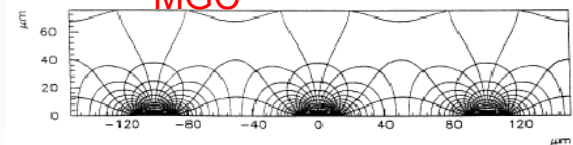
1



5



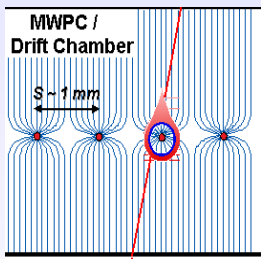
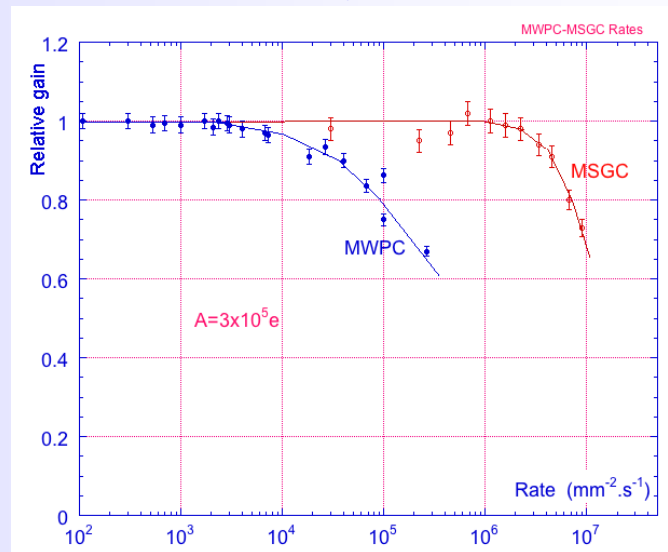
10



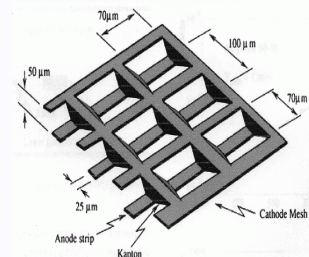
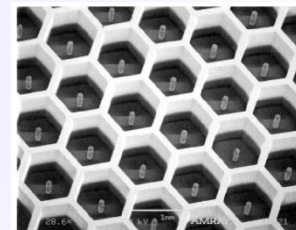
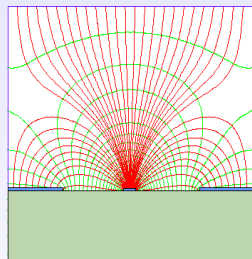
R. Bellazzini et al.

Semiconductor Industry technology:

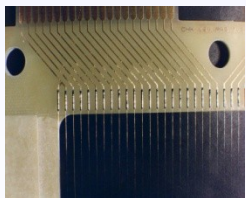
- Photolithography
- Etching
- Coating
- Doping



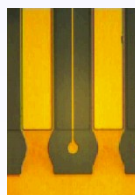
Amplifying cell
reduction by
factor of 10



Operational instabilities:

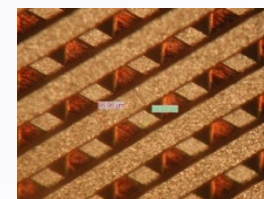
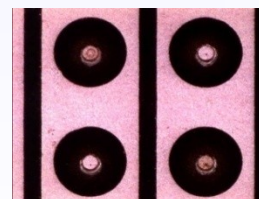


Rate Capability $> 10^6/\text{mm}^2$
Position Resolution $\sim 40\mu\text{m}$
2-track Resolution $\sim 400\mu\text{m}$



MSGC

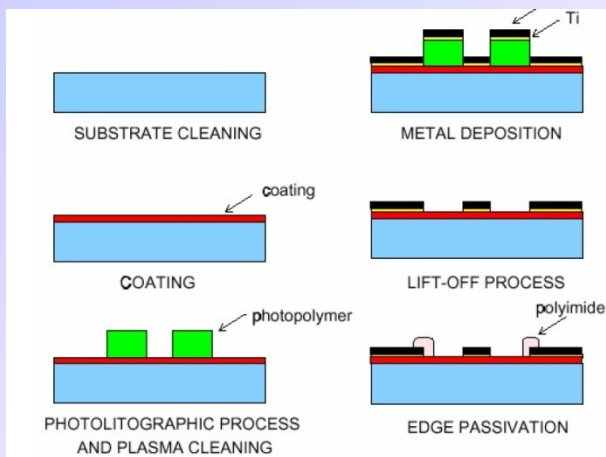
Substrate charging-up
Discharges
Polymer deposition (ageing)



MWPC



Anton Oed

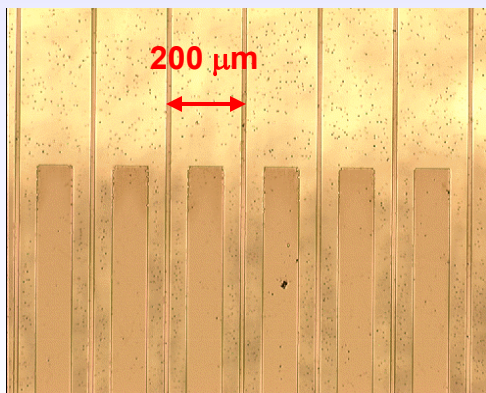
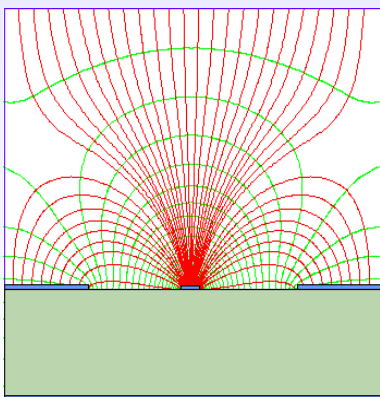


Thin metal anodes and cathodes on insulating support (glass, flexible polyimide ..)

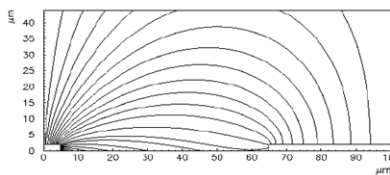
Problems:

High discharge probability under exposure to highly ionizing particles caused by the regions of very high E field on the border between conductor and insulator.

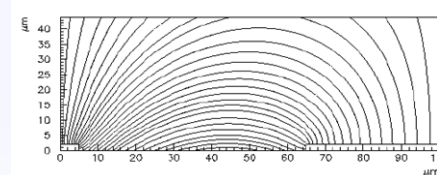
Charging up of the insulator and modification of the E field → time evolution of the gain.



insulating support



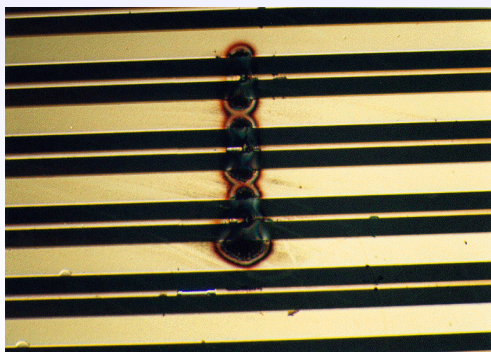
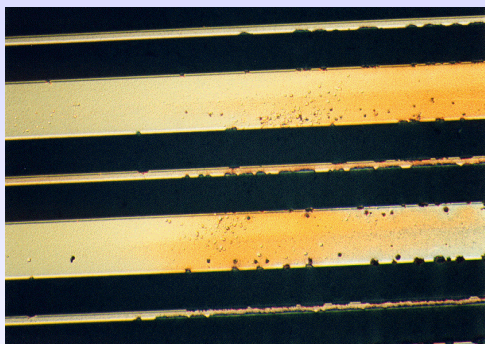
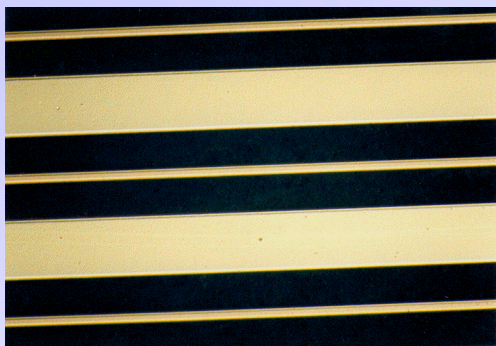
slightly conductive support



R. Bellazzini et al.

Solutions:

slightly conductive support
multistage amplification



Surface charging

Bulk resistivity of the support material

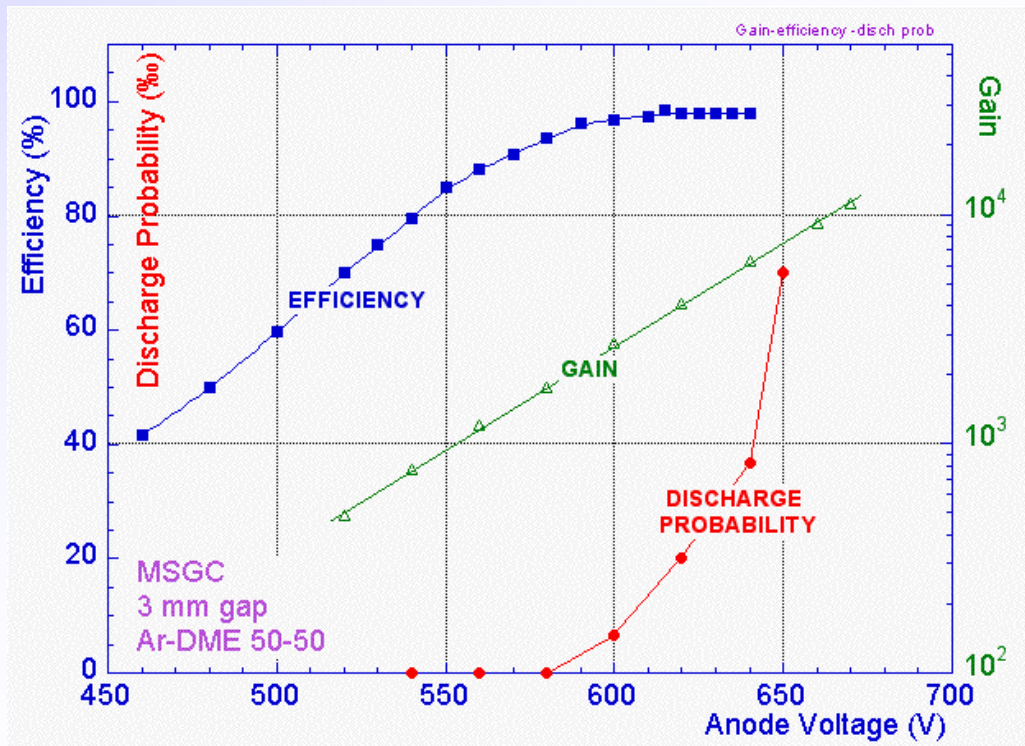
Surface modification by doping or deposition

Ageing

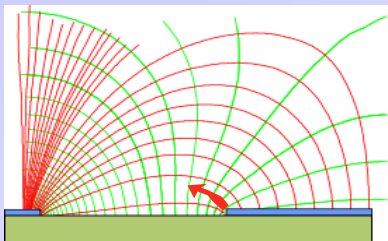
Gas, Gas system, MSGC support,

Construction material

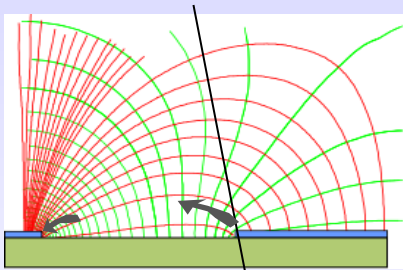
Discharges



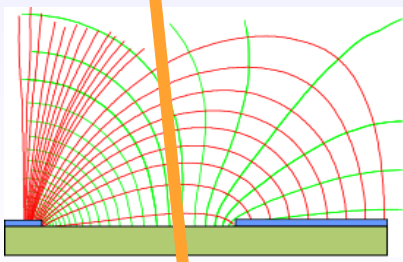
MSGC: Discharge mechanisms



Field emission from the cathode edge

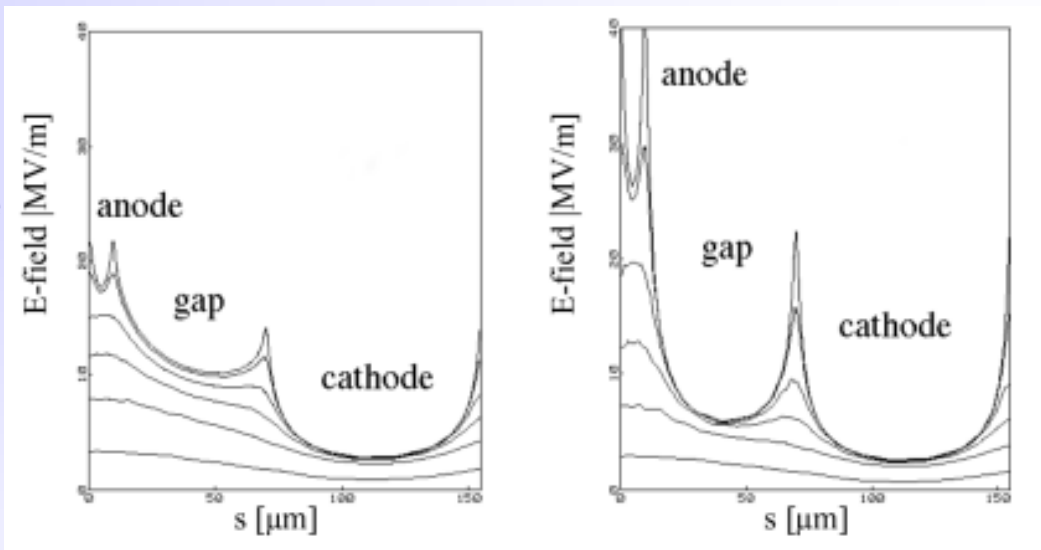


Charge pre-amplification for ionization released in high field close to cathode



Very high ionization release:
avalanche size exceeds Reather's limit

Electric field strength close to support plane in MSGC

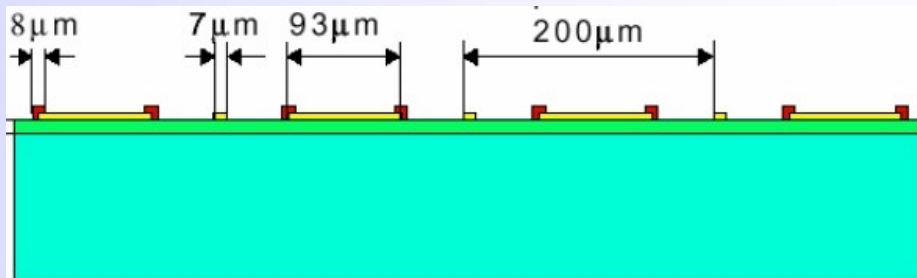


Coated MSGC

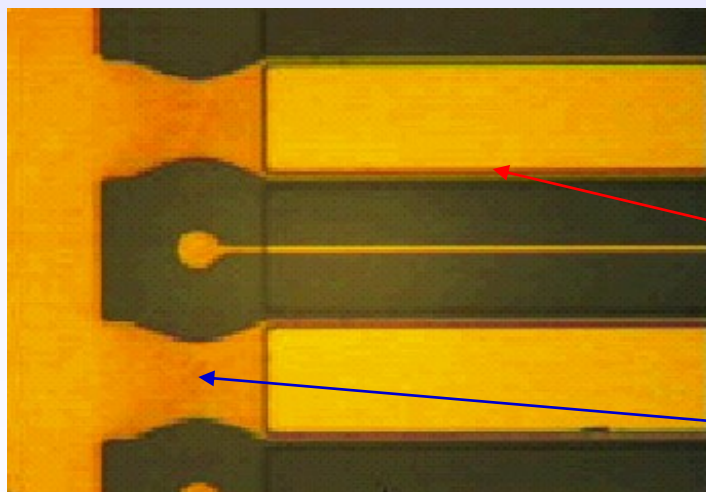
Uncoated MSGC

Surface resistivity modification

Cathode edge passivation

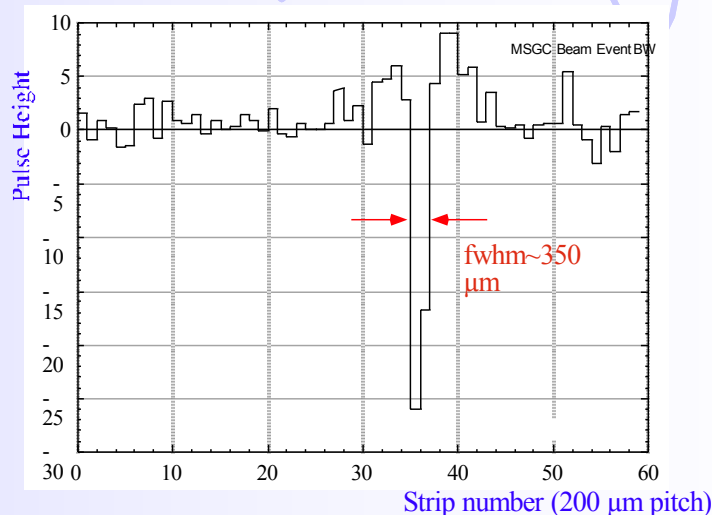
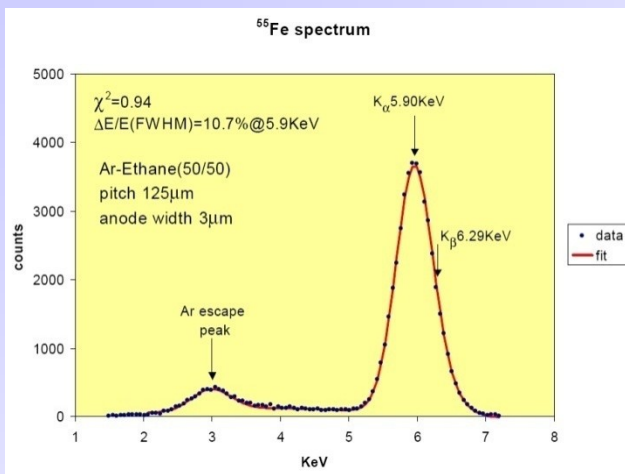


- advanced passivation: polyimide ($2\mu\text{m}$)
- metal: gold ($0.6\text{-}0.8\mu\text{m}$)
- undercoating: Pestov or S8900 glass ($0.5\text{-}1\mu\text{m}$)
- substrate: Desag glass ($300\ \mu\text{m}$)



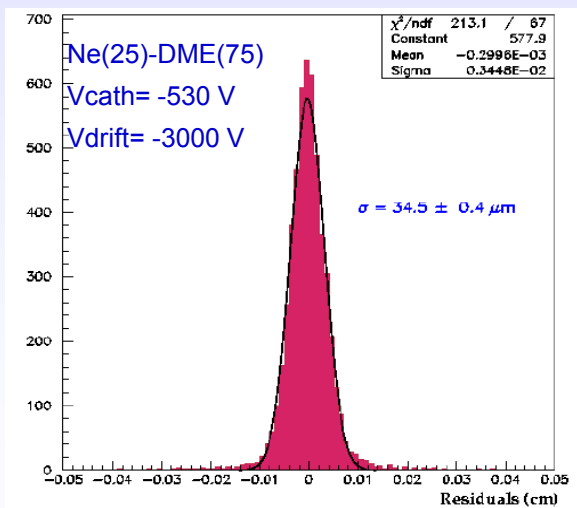
Advanced passivation

Standard passivation



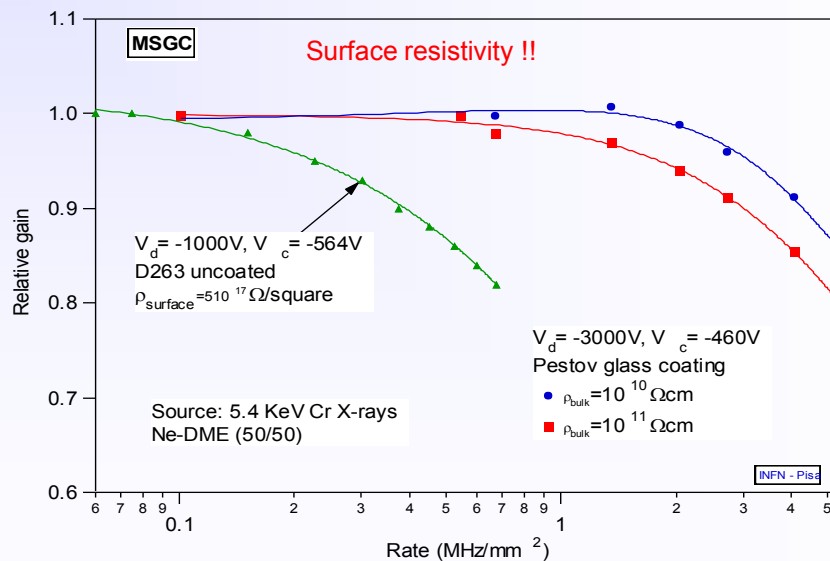
Energy resolution ~11% for 5.9 keV

Single event wire map



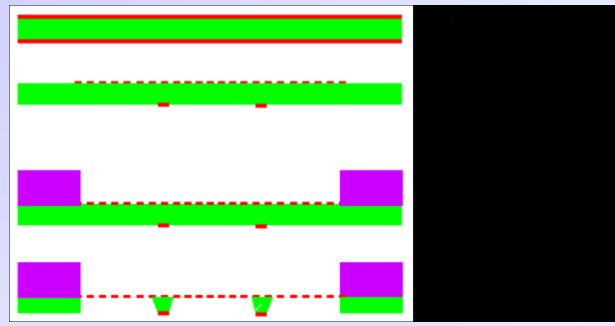
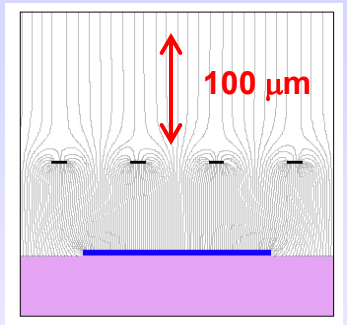
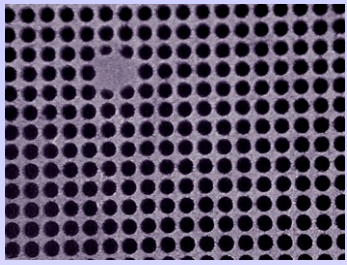
Spatial resolution = $34.5 \pm 0.4\ \mu\text{m}$

2-track resolution ~400 μm

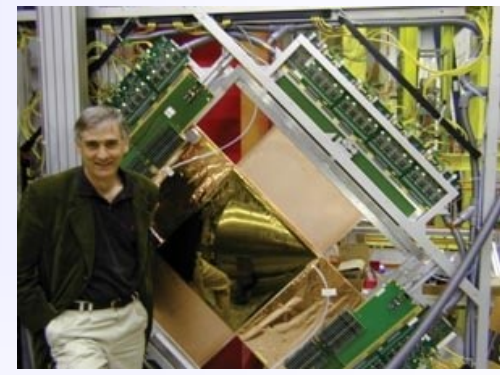
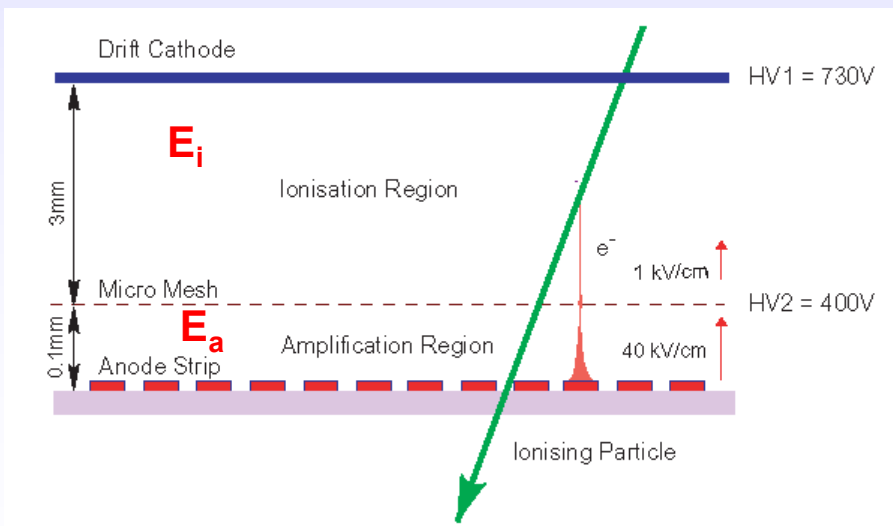


Rate capability > 1 MHz/mm^2

Micromegas – Micromesh Gaseous Structure



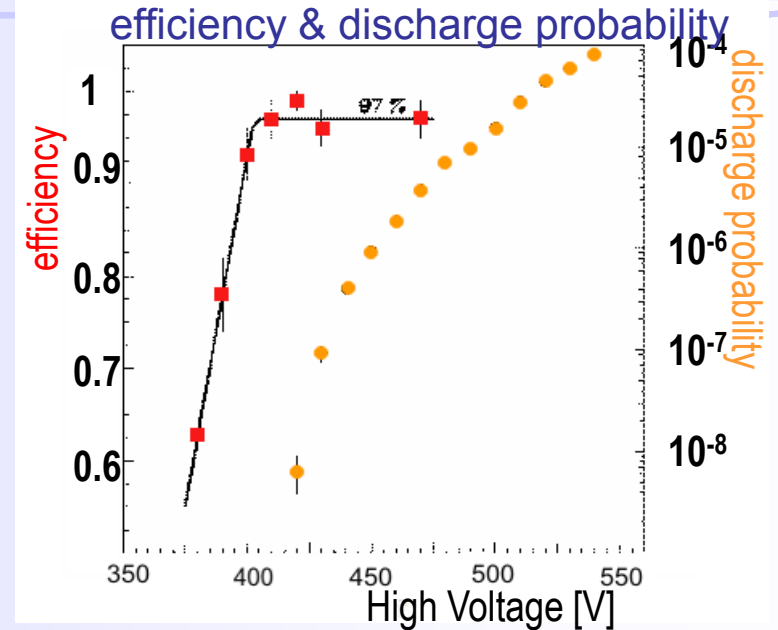
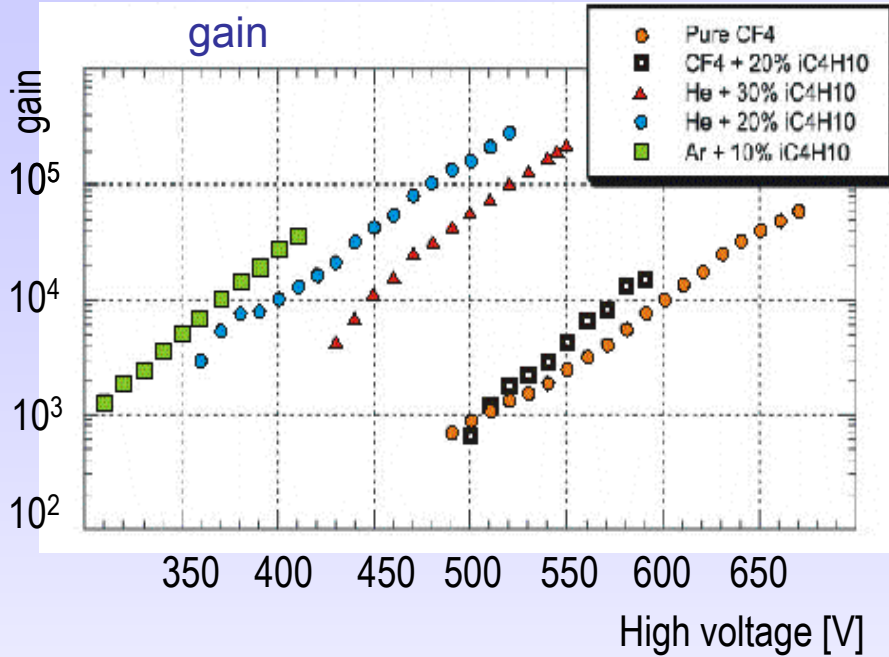
Micromesh mounted above readout structure (typically strips).
E field similar to parallel plate detector.
 $E_a/E_i \sim 50$ to secure electron transparency and positive ion flowback suppression.



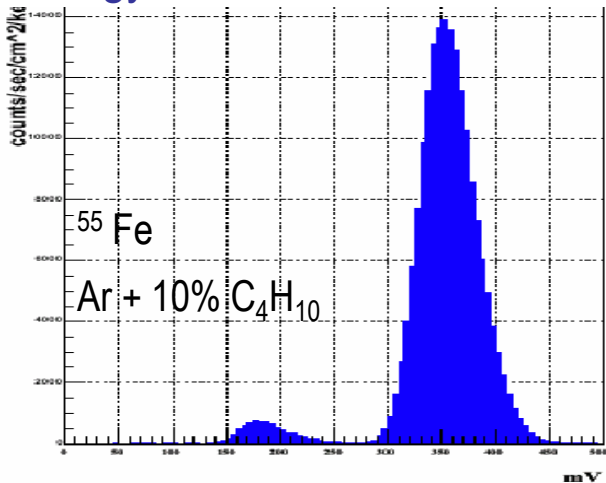
Ioannis Giomataris

Y.Giomataris et al, NIM A 376 (1996) 29

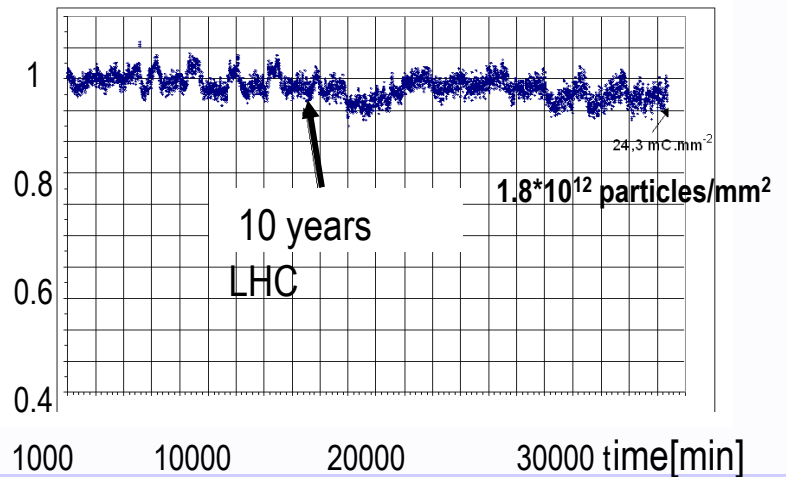
Micromegas – Micromesh Gaseous Structure



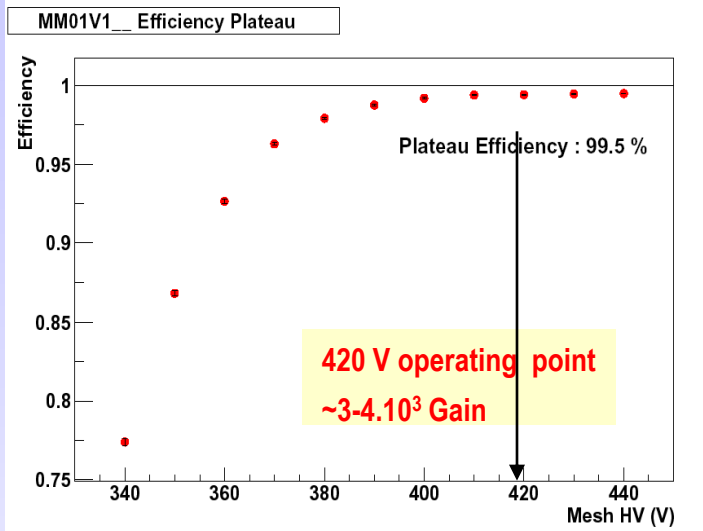
energy resolution ~ 10%



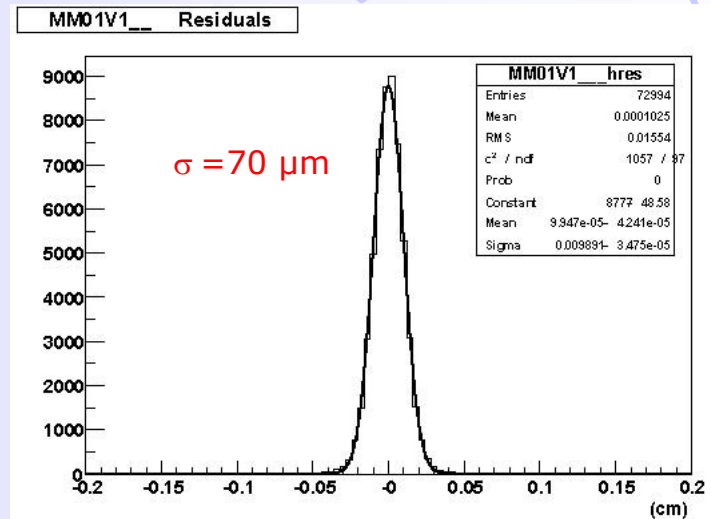
ageing: Ar-iC₄H₁₀ 94-6% up to 24.3mC/mm²



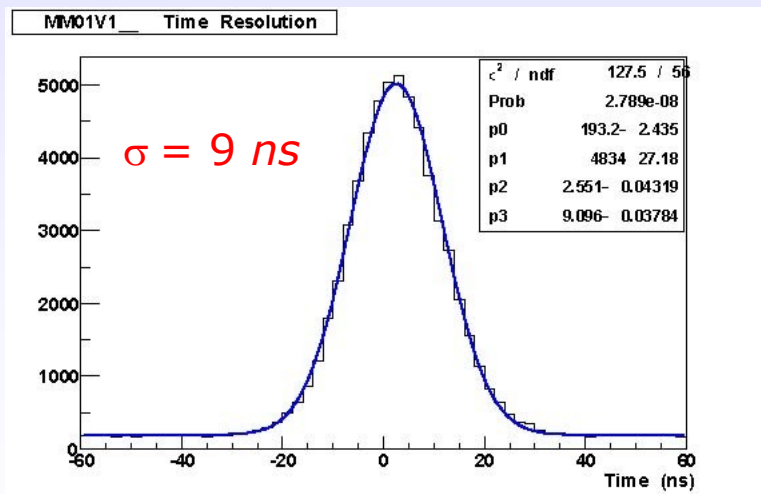
Micromegas – Micromesh Gaseous Structure



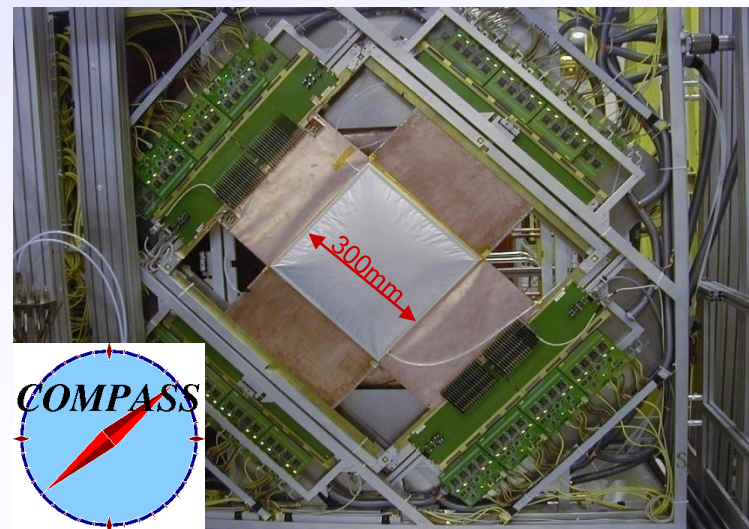
Large efficiency plateau > 40 V

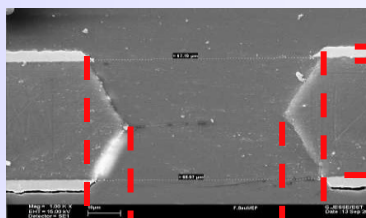
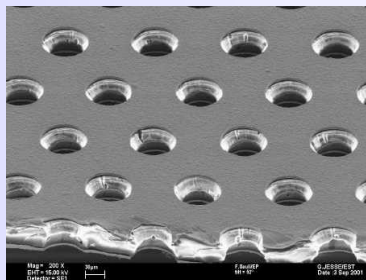
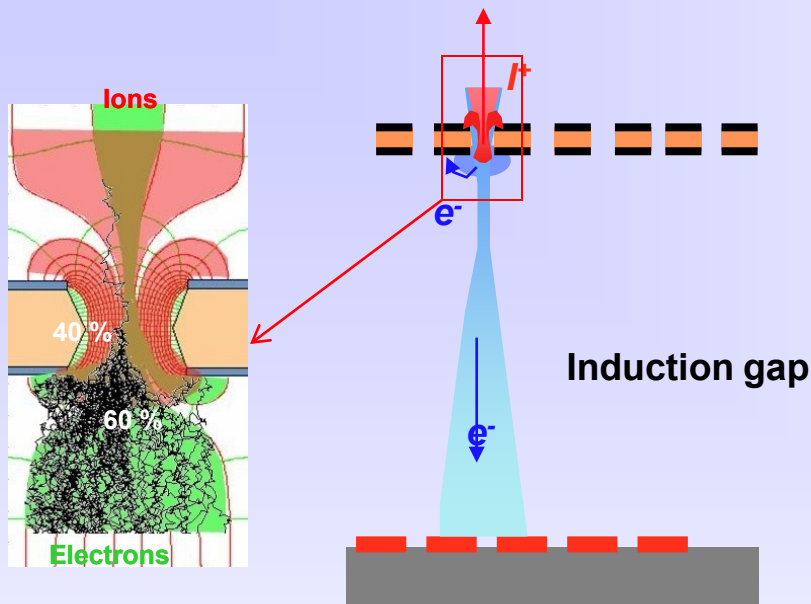


Spatial resolution < 70 μm

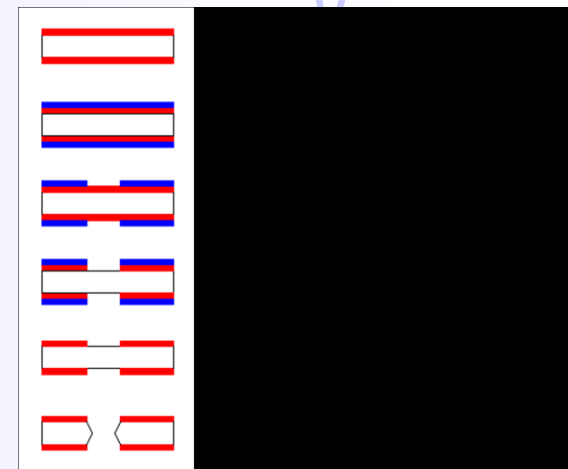


Time resolution : 9 ns



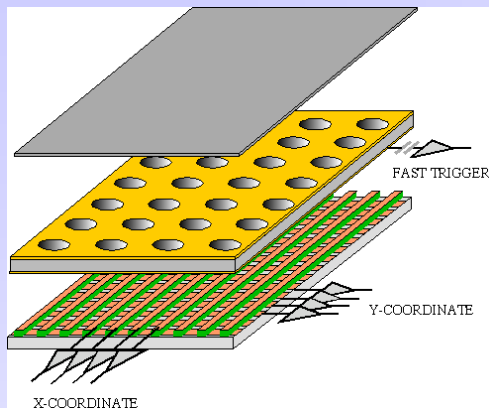


5 μm
50 μm
55 μm
70 μm



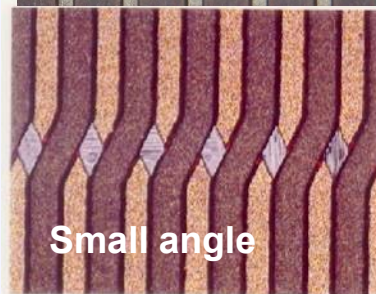
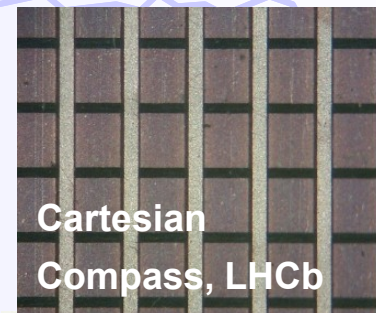
Thin, metal coated polyimide foil perforated with high density holes.

Electrons are collected on patterned readout board.
A fast signal can be detected on the lower GEM electrode for triggering or energy discrimination.
All readout electrodes are at ground potential.
Positive ions partially collected on the GEM electrodes.

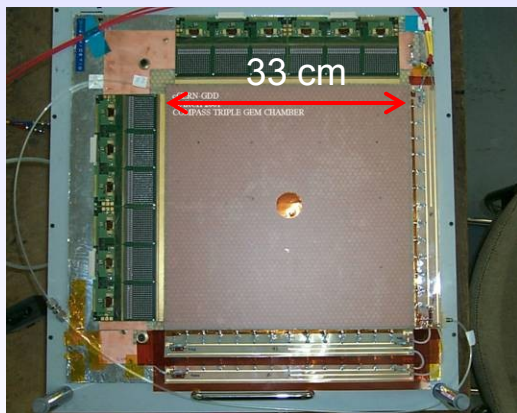


Full decoupling of the charge amplification structure from the charge collection and readout structure.

Both structures can be optimized independently !



A. Bressan et al, Nucl. Instr. and Meth. A425(1999)254

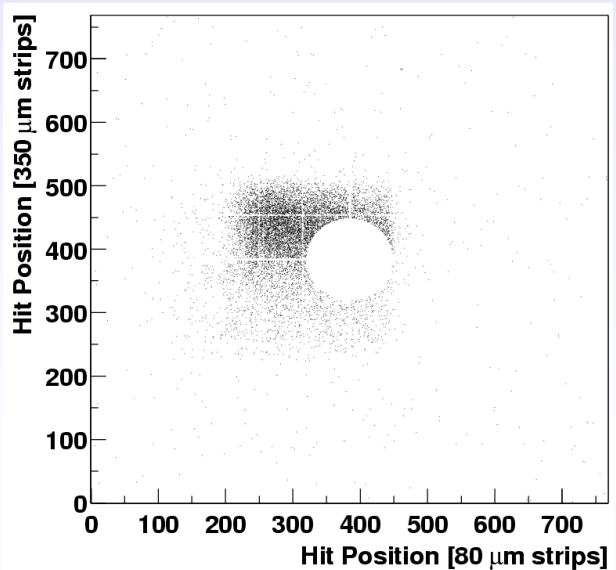
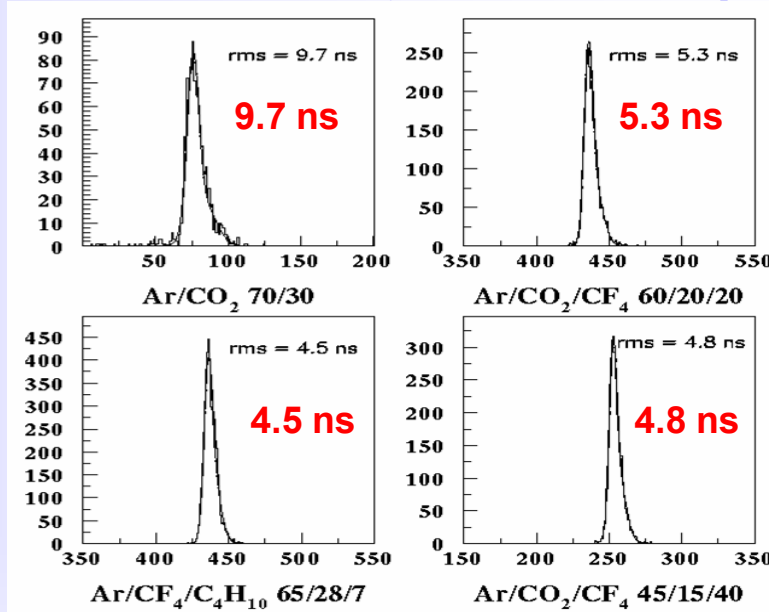
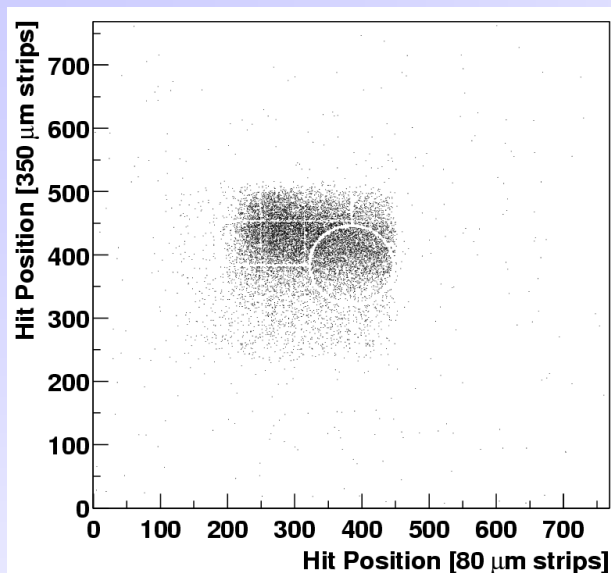


Compass

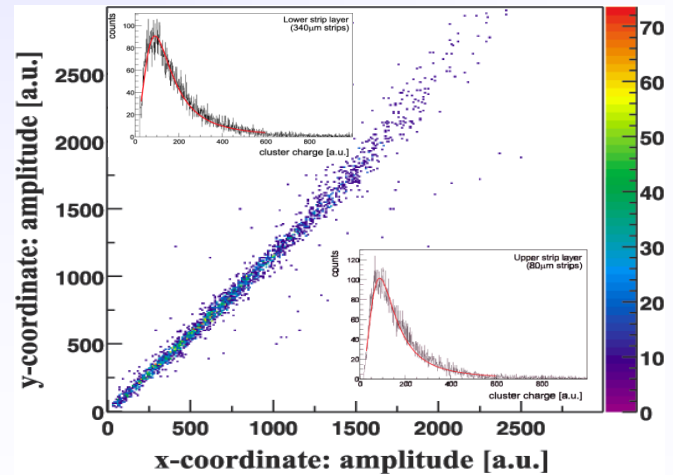


Totem

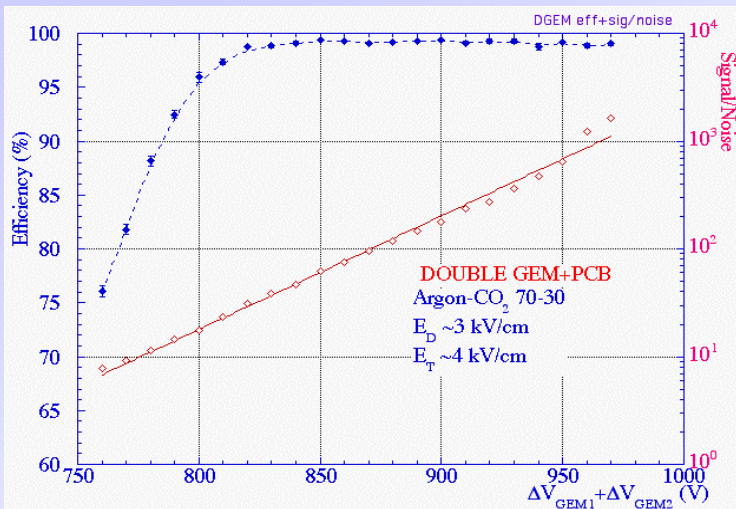
Both detectors use three GEM foils in cascade for amplification to reduce discharge probability by reducing field strength.



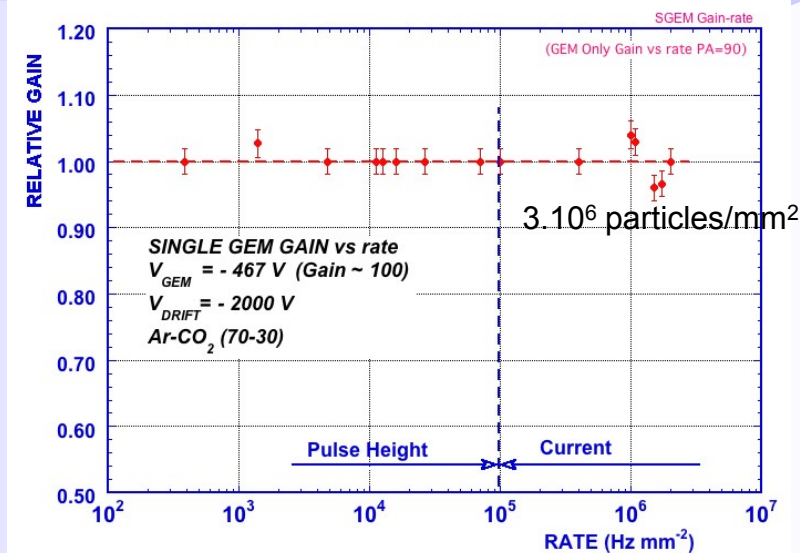
Time resolution



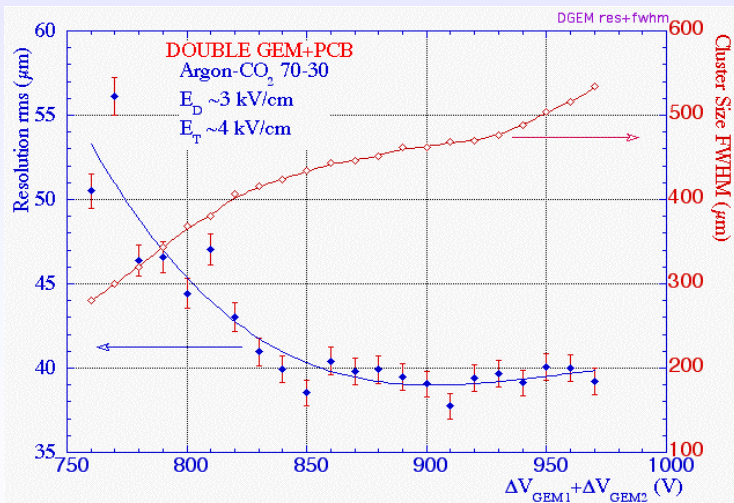
Charge correlation (cartesian readout)



Efficiency for minimum ionizing particles with 3 mm gap

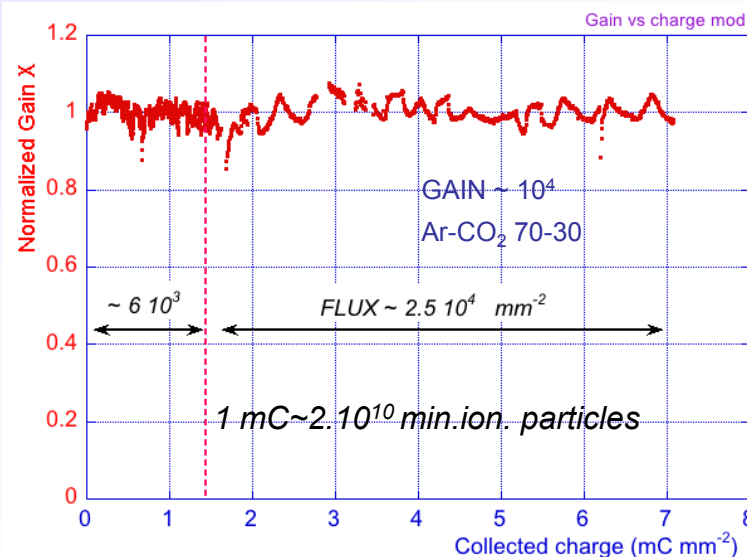


Rate capability > 10⁶ Hz mm⁻²



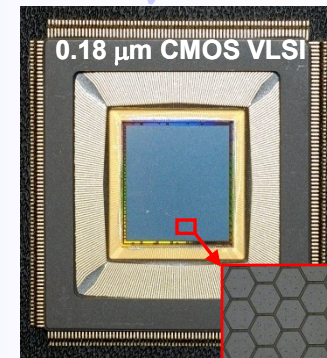
Space resolution ~ 40 μ m rms

Cluster size ~ 500 μ m FWHM

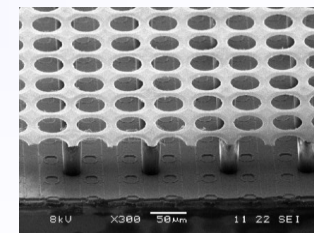
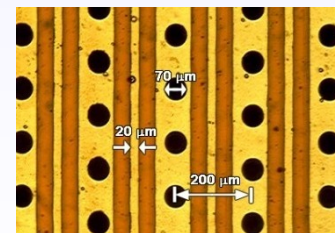
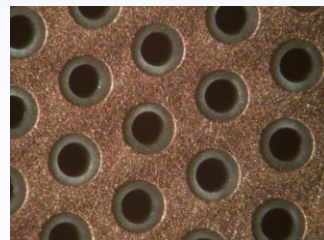
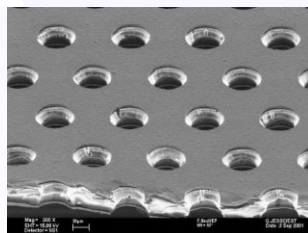
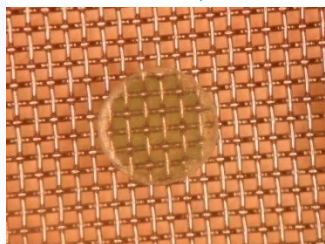
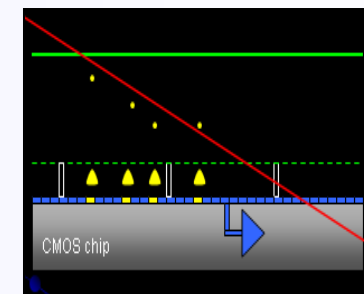
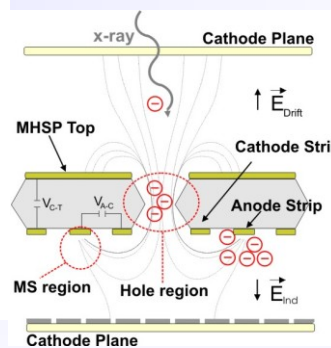
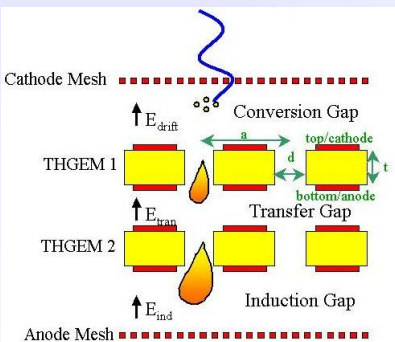
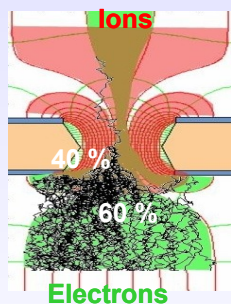
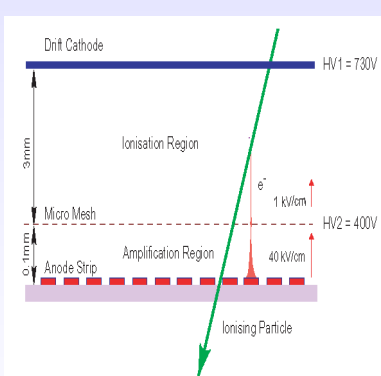


C. Altunbas et al, DESY Aging Workshop (Nov. 2001) Nucl. Instr. and Meth. A
J. Benloch et al, IEEE NS-45(1998)234

- MSGC
- Micromegas
- GEM
- Thick-GEM, Hole-Type Detectors and RETGEM
- MPDG with CMOS pixel ASICs
- Ingrid Technology



CMOS high density readout electronics



Micromegas

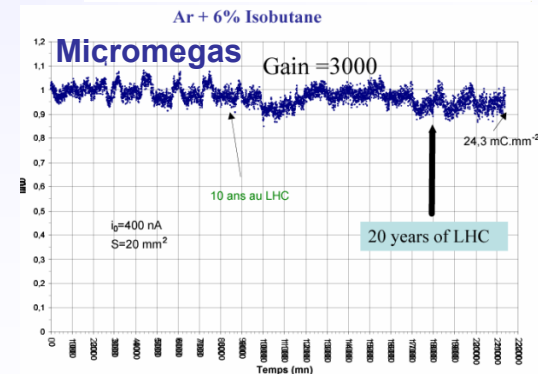
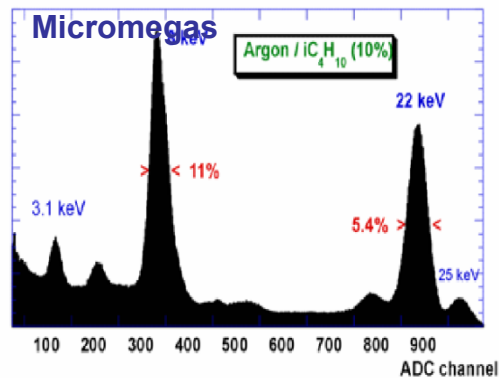
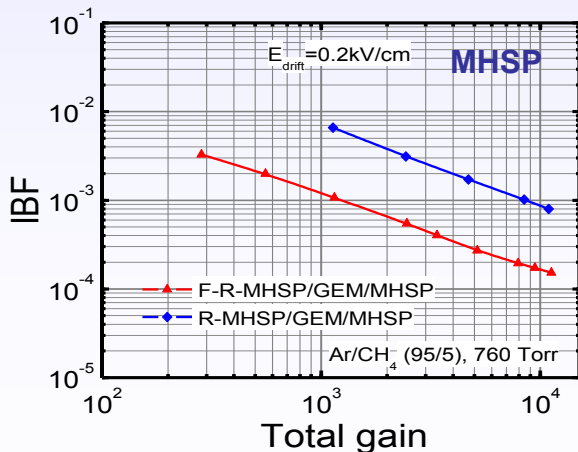
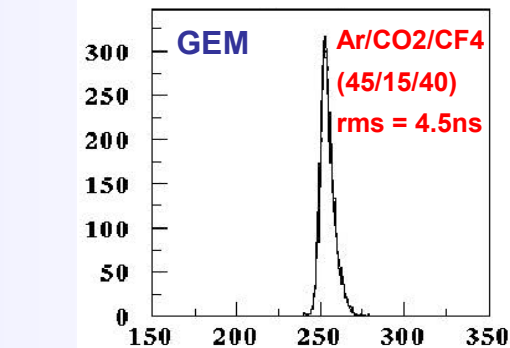
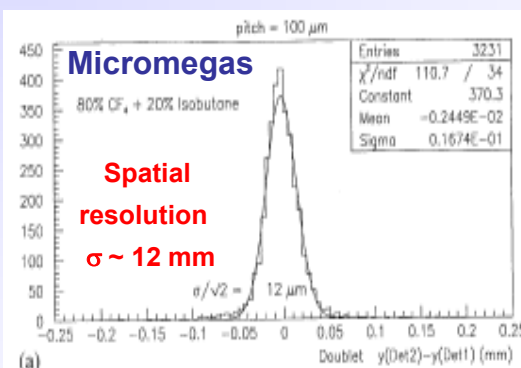
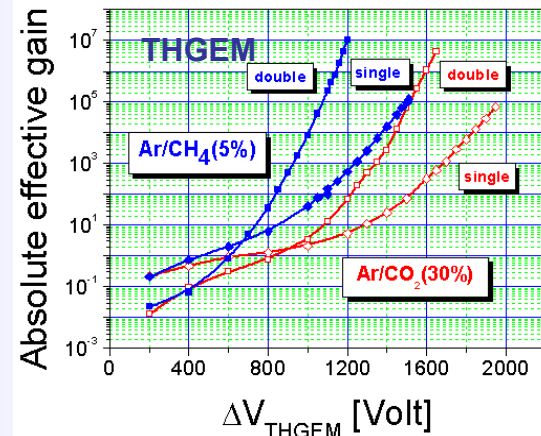
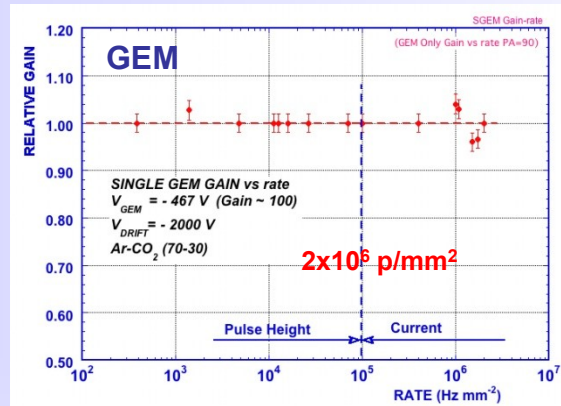
GEM

THGEM

MHSP

Ingrid

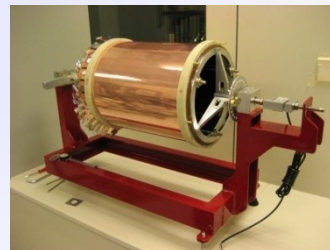
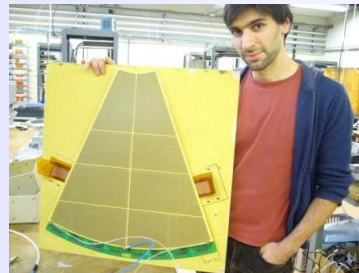
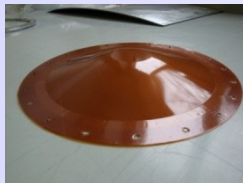
- Rate Capability
- High Gain
- Space Resolution
- Time Resolution
- Energy Resolution
- Ageing Properties
- Ion Backflow Reduction
- Photon Feedback Reduction



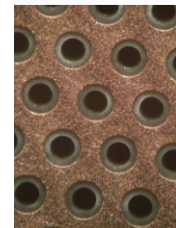
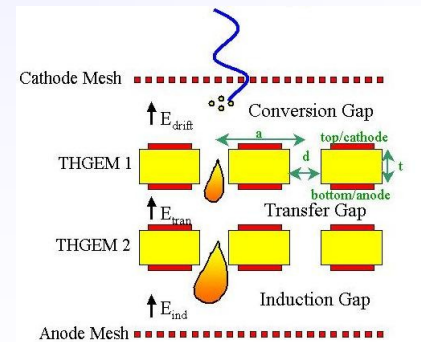
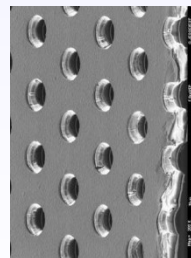
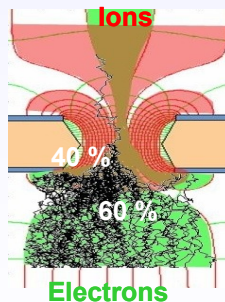
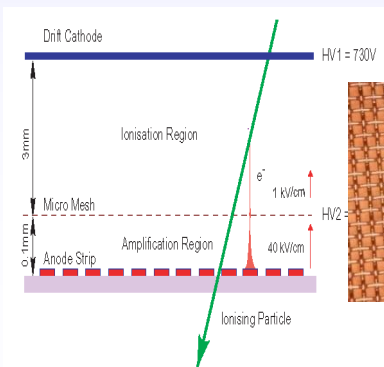
Bulk Micromegas



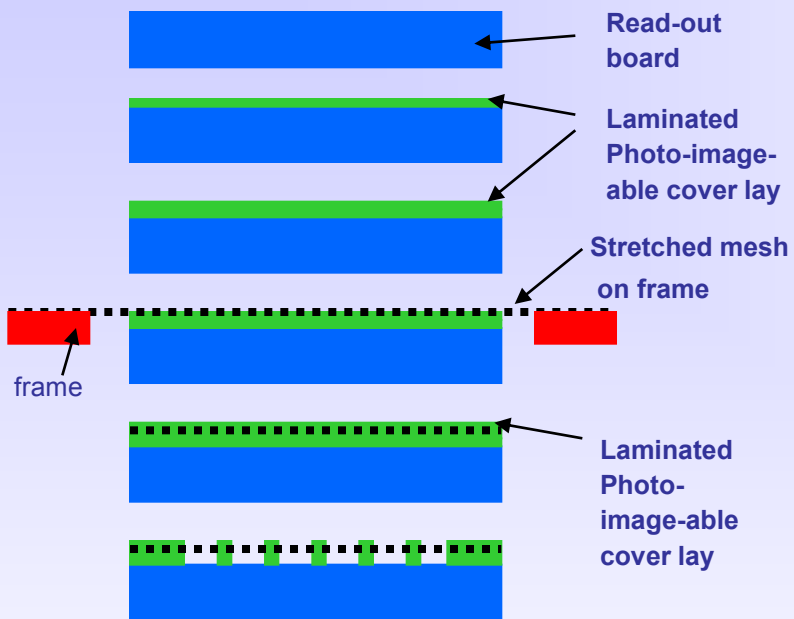
Single mask GEM



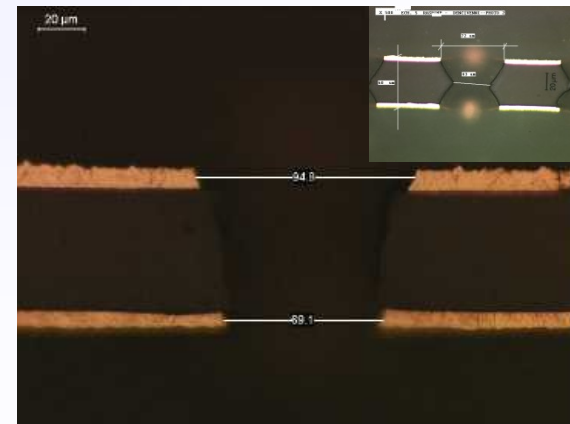
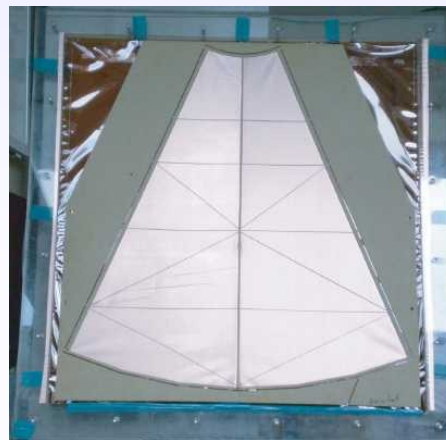
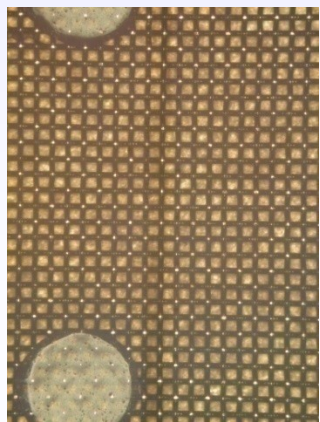
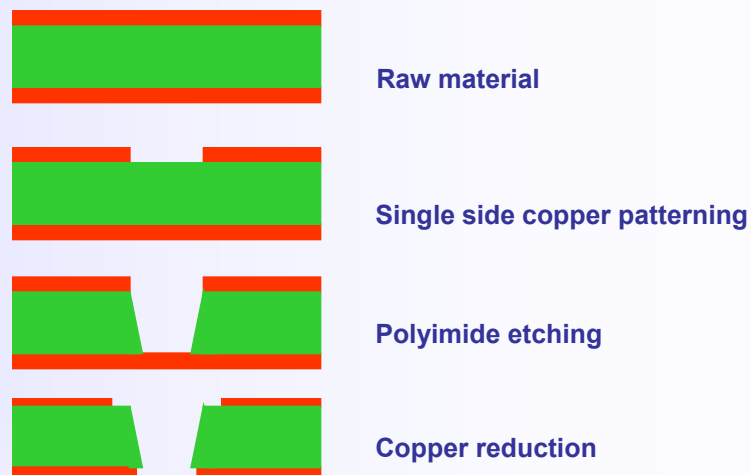
THGEM



Bulk Micromegas



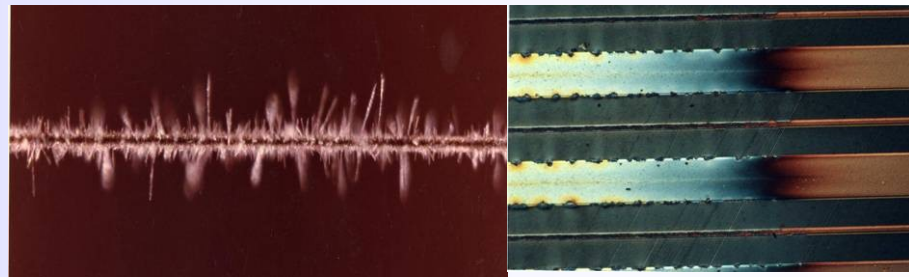
Single mask GEM



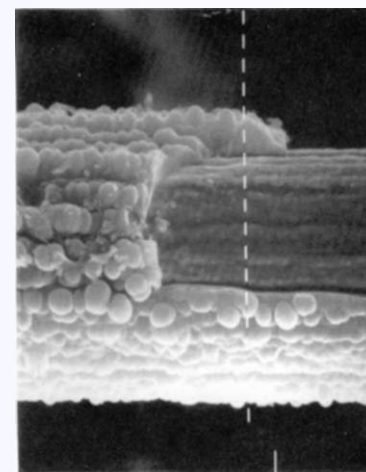
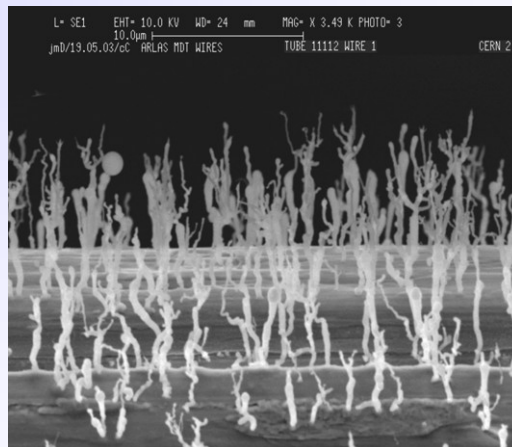
Classical ageing

Avalanche region → plasma formation
(complicated plasma chemistry)

- Dissociation of detector gas and pollutants
- Highly active radicals formation
- Polymerization (organic quenchers)
- Insulating deposits on anodes and cathodes



Anode: increase of the wire diameter, reduced and variable field, variable gain and energy resolution.



Cathode: formation of strong dipoles, field emission and microdischarges (Malter effect).



Solutions: careful material selection for the detector construction and gas system, detector type (GEM is resistant to classical ageing), working point, non-polymerizing gases, additives suppressing polymerization (alcohols, methylal), additives increasing surface conductivity (H₂O vapour), cleaning additives (CF₄).

Creation of database of "radiation-hard" materials & detectors depending on application, commercially available materials

Source	Product	Outgas	Effect in G.D.	Note
CERN/GDD	STYCAST 1266 (A+B)	NO	NO	Long curing time
HERA-B/OTR	STYCAST 1266 (A+Catalyst 9)	NO	NO	In Use
CERN/GDD	HEXCEL EPO 93L	NO	NO	Out of production
HERA-B/ITR	ECCOBOND 285	NO	NO	In Use
CERN/GDD ATLAS/TRT	ARALDITE AW103 (Hardener HY 991)	NO	NO	In Use
ATLAS/TRT	TRABOND 2115	NO	NO	In Use

Low Outgassing room-T epoxies

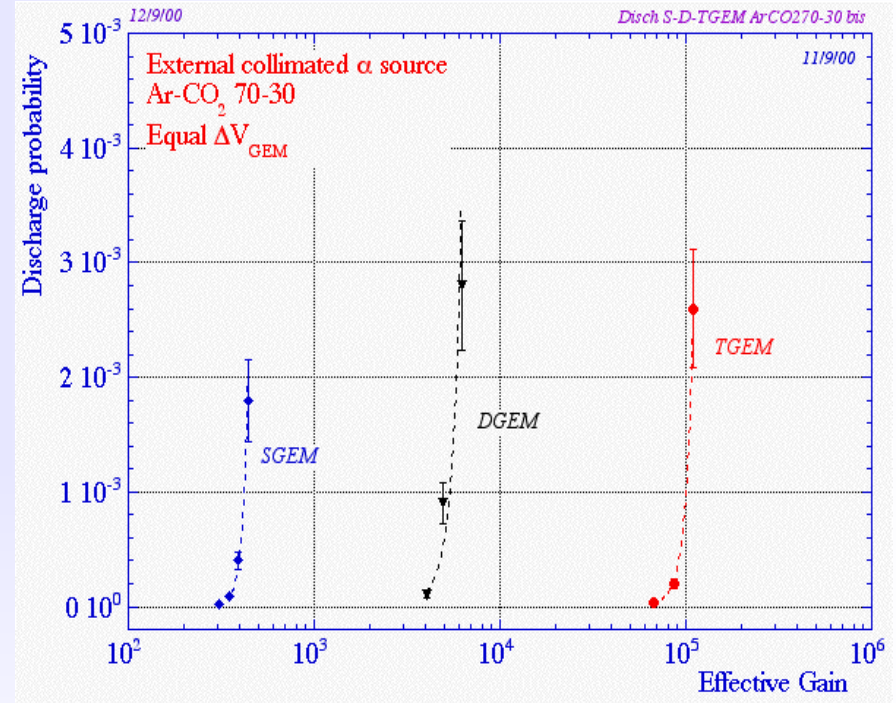
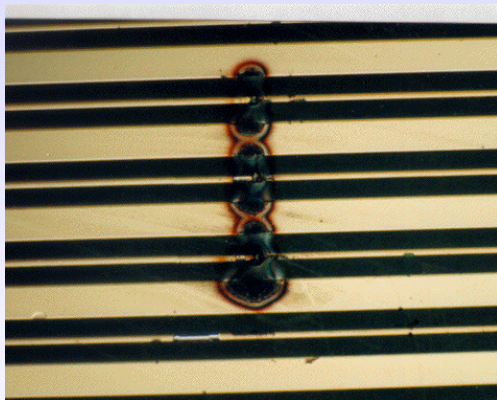
Source	Product	Outgas	Effect in G.D.	Result
CERN/GDD ATLAS/TRT	ARALDITE AW 106 (Hardener HV 935 U)	YES		BAD
CERN/GDD	DURALCO 4525	YES	YES	BAD
CERN/GDD	DURALCO 4461	YES	YES	BAD
CERN/GDD	HEXCEL A40	YES	-	BAD
CERN/GDD	TECHNICOLL 8862 + (Hardener 8263)	YES	-	BAD
CERN/GDD	NORLAND NEA 155	YES	-	BAD
CERN/GDD	EPOTEK E905	YES	-	BAD
CERN/GDD	NORLAND NEA 123 (UV)	YES	-	BAD

Outgassing room-T epoxies

Discharges

Field and charge density dependent effect.

Solution: multistep amplification
resistive electrodes



Insulator charging up resulting in gain variable with time and rate

Solution: slightly conductive materials

MAXWELL (*Ansoft*)

electrical field maps in 2D& 3D, finite element calculation for arbitrary electrodes & dielectrics

HEED (*I.Smirnov*)

energy loss, ionization

MAGBOLTZ (*S.Biagi*)

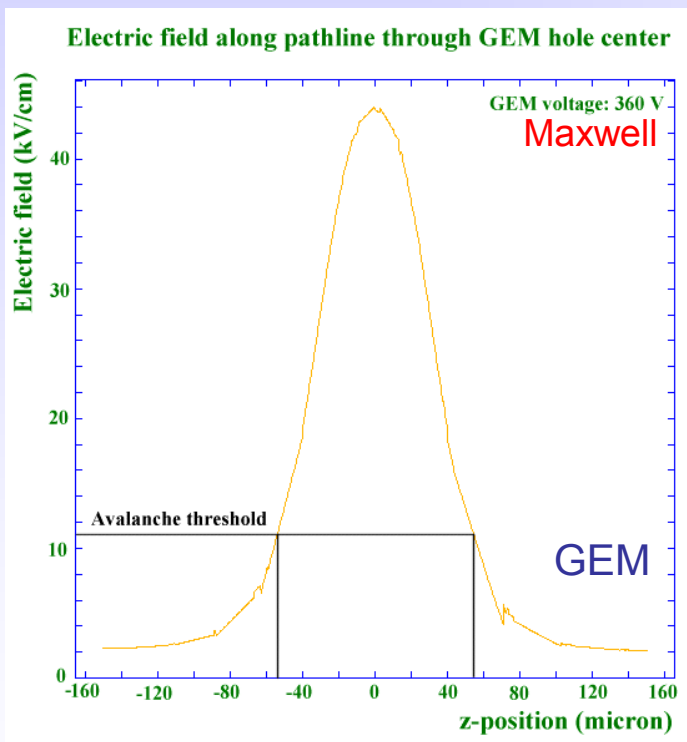
electron transport properties: drift, diffusion, multiplication, attachment

Garfield (*R.Veenhof*)

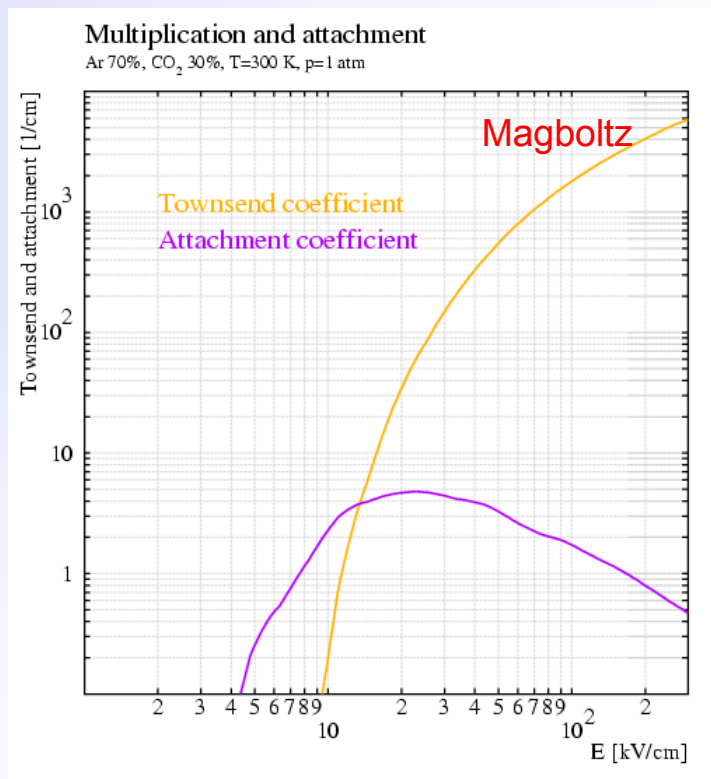
fields, drift properties, signals (interfaced to programs above)

PSpice (*Cadence D.S.*) electronic signal

Input: detector geometry, materials and electrodes potentials, gas cross sections.

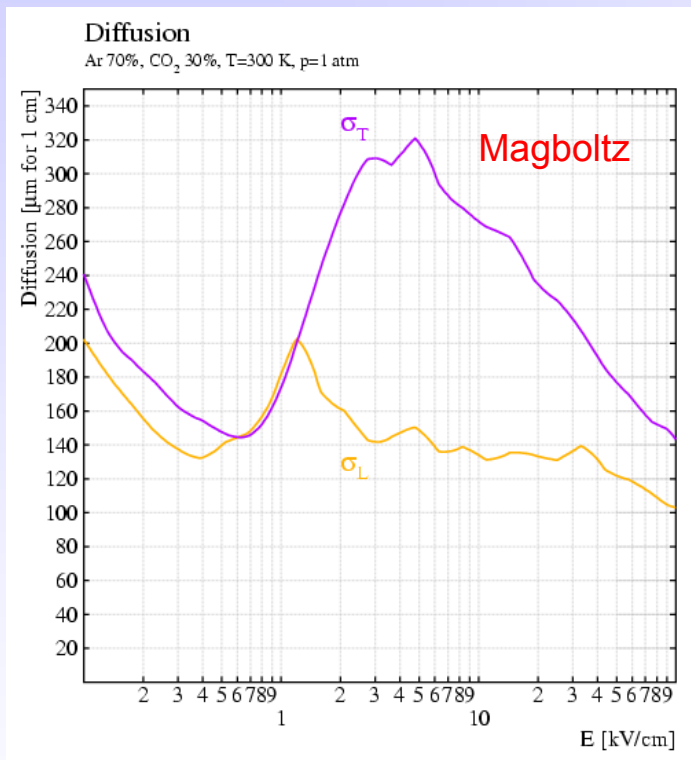


Field Strength

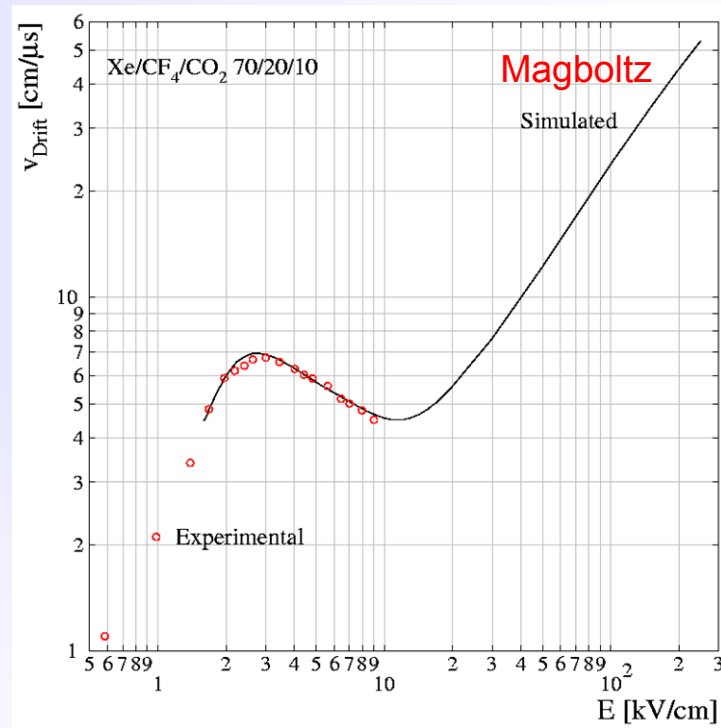


Townsend coefficient

P. Cwetanski, <http://pcwetans.home.cern.ch/pcwetans/>



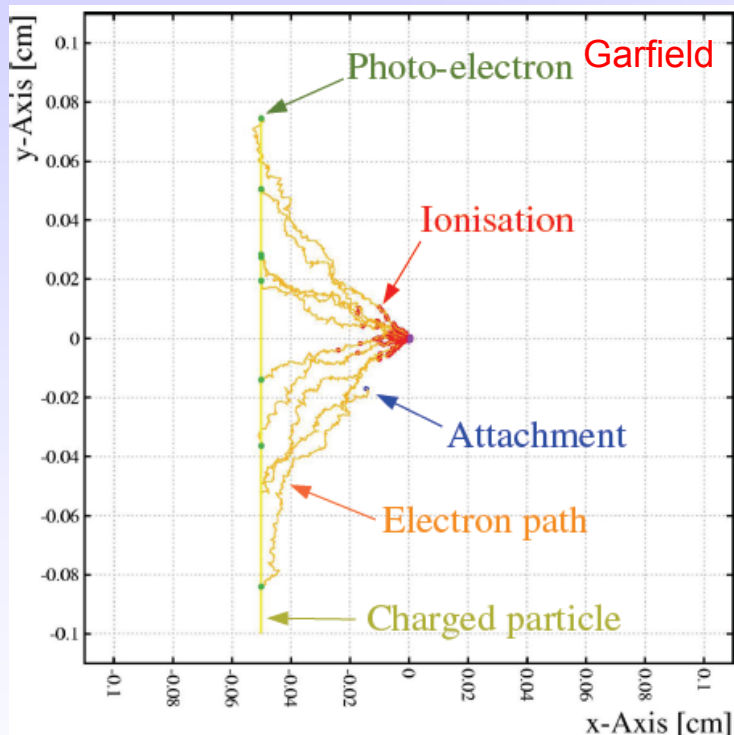
Longitudinal, transverse diffusion



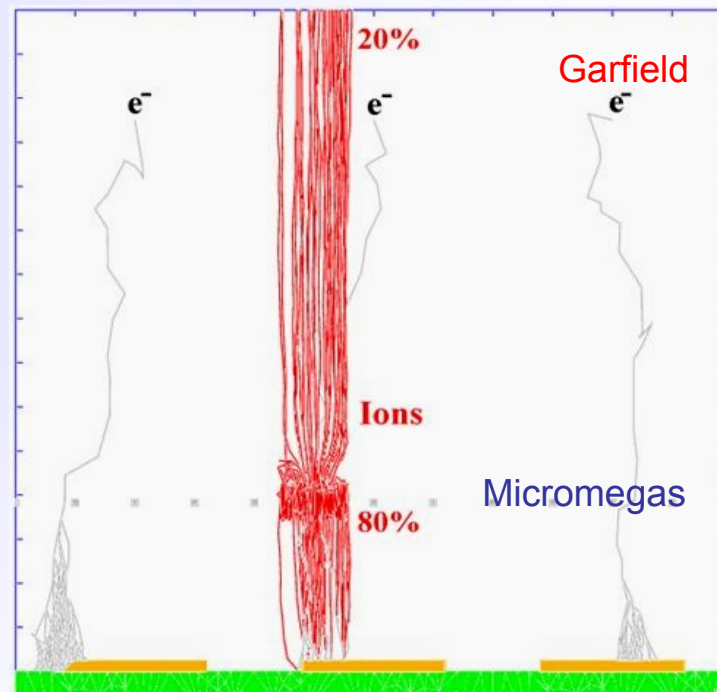
Drift velocity

P. Cwetanski, <http://pcwetans.home.cern.ch/pcwetans/>

R. Veenhof – CERN detector seminar



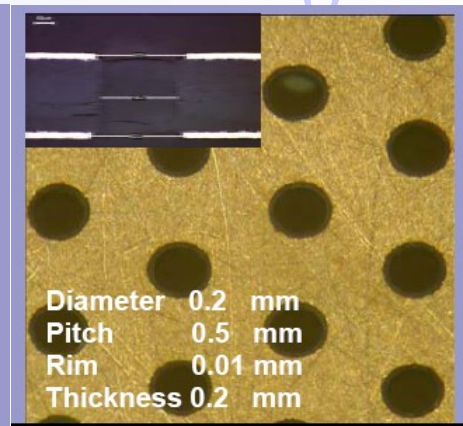
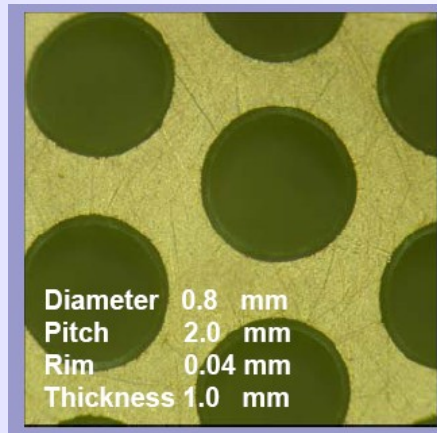
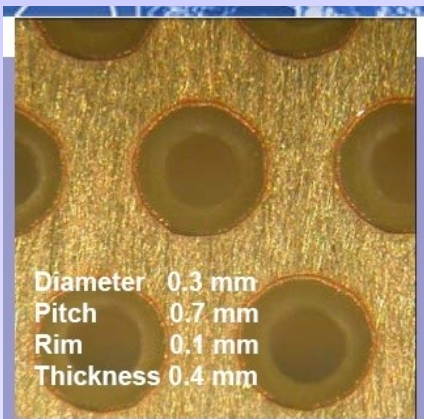
CSC-microtracking in Garfield



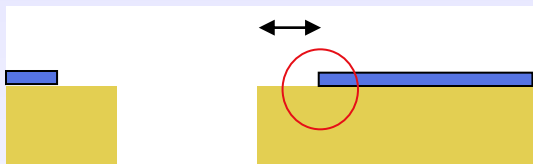
Positive ion backflow

Conclusion: we don't need to built detector to know its performance

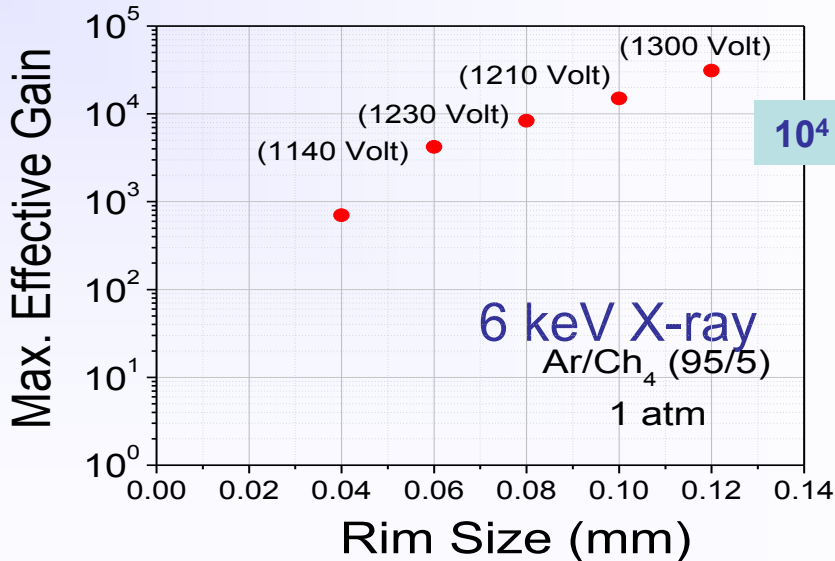
THGEM Example



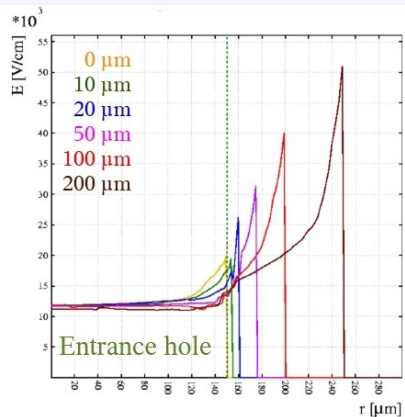
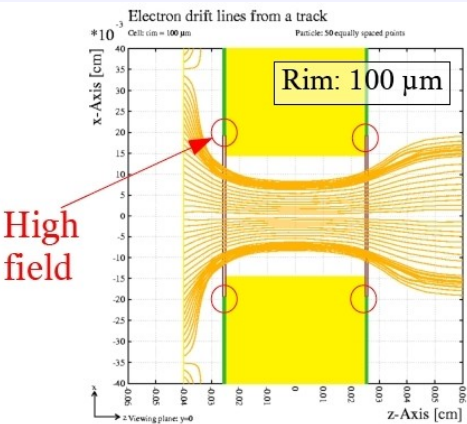
Mask etching + drilling; rim = 0.1mm

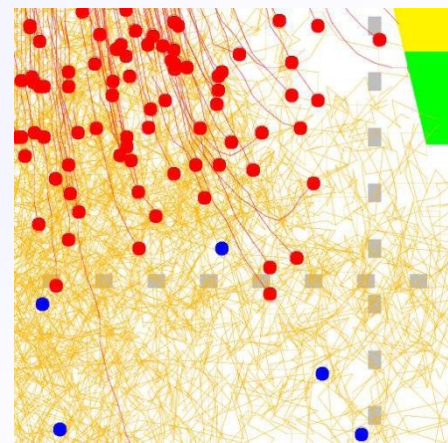
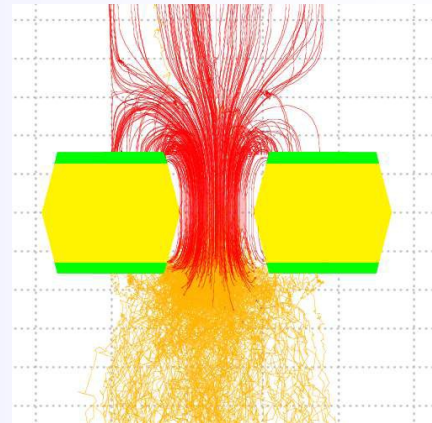
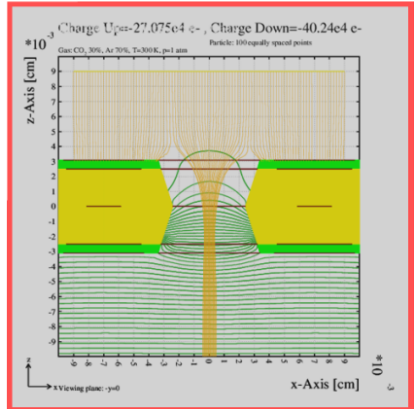
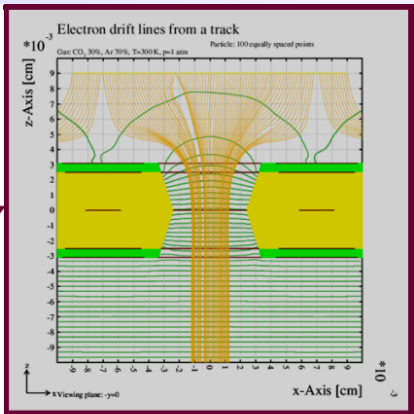
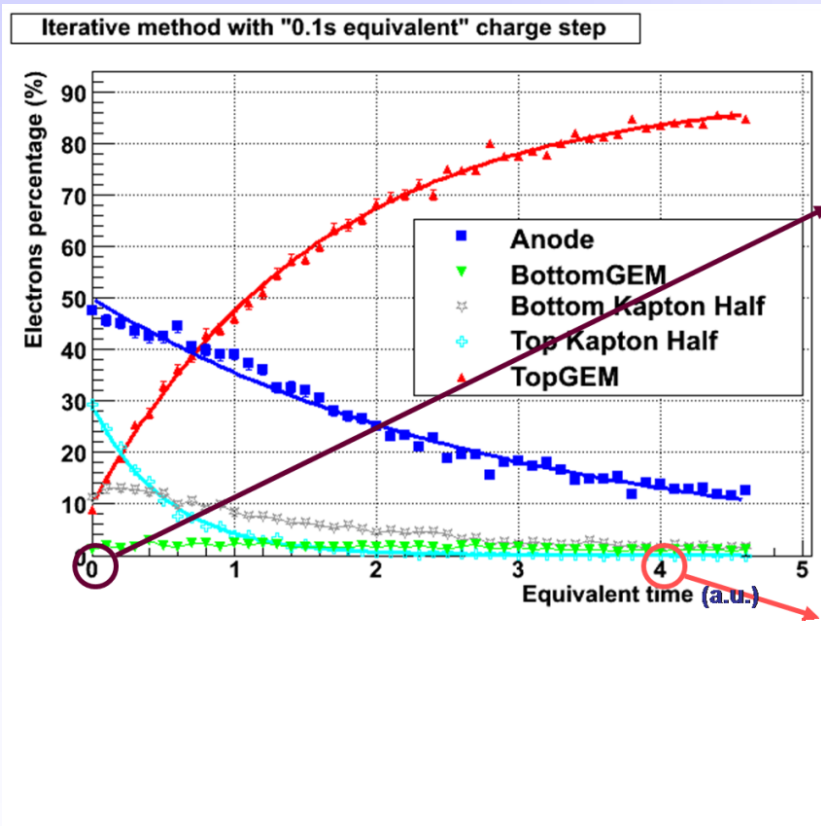


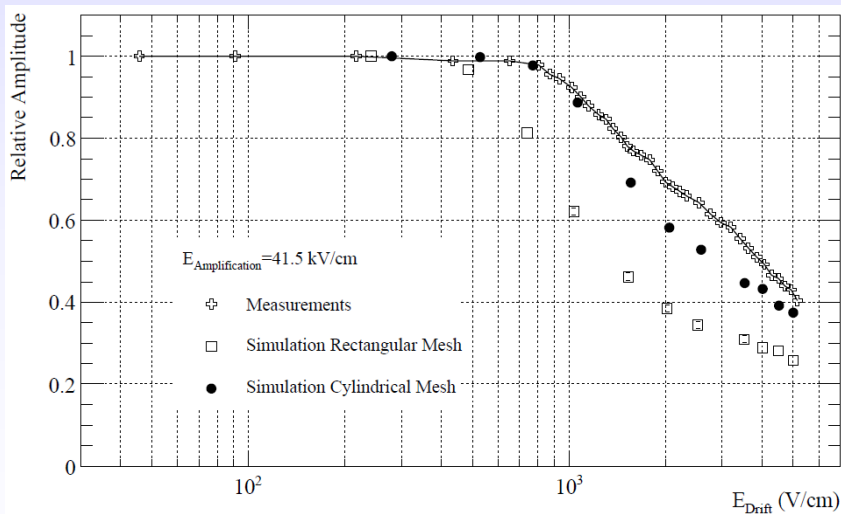
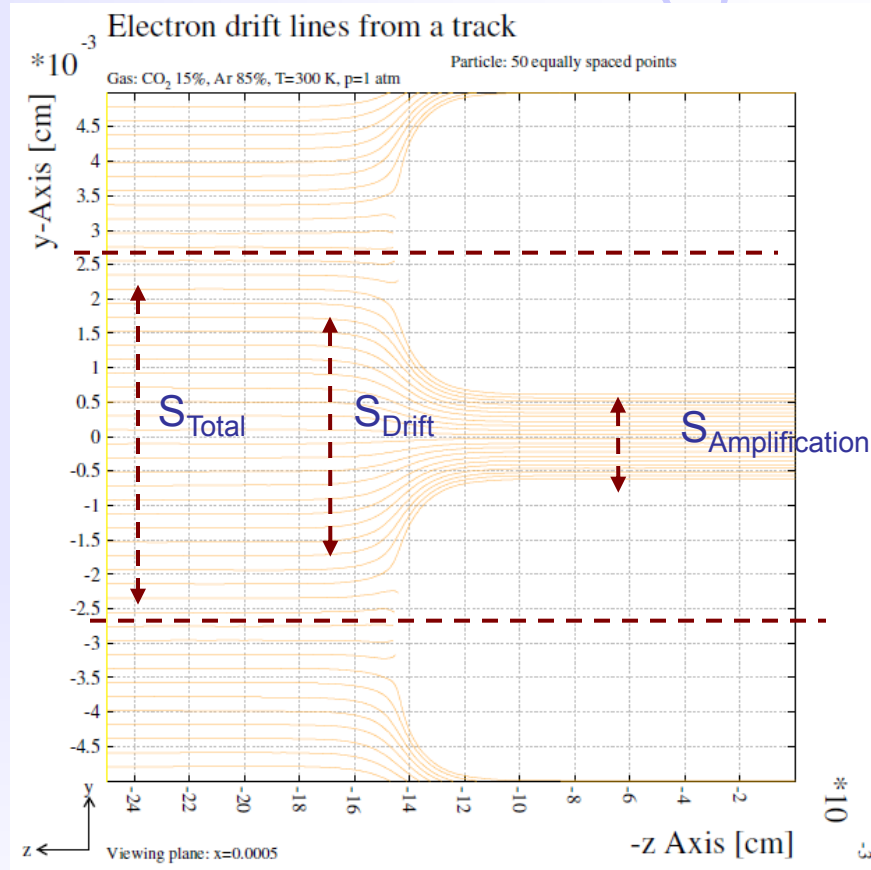
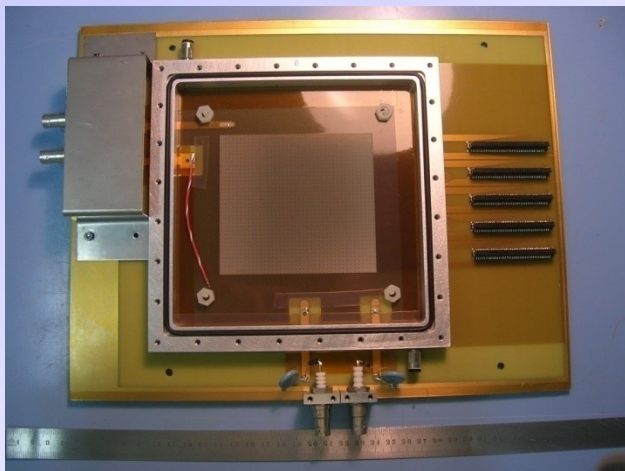
Drilling + chemical rim etching without mask



pitch = 1 mm; diameter = 0.5 mm;
 rim = 40; 60; 80; 100; 120 μ m







$$P(e\text{-collection}) = \frac{S_{Drift}}{S_{Total}}$$

$$= \frac{S_{Amplification} \times \text{Field-Ratio}}{S_{Total}}$$

$$\sim (\text{hole diameter})^2 \quad \sim (\text{wires pitch})^2$$

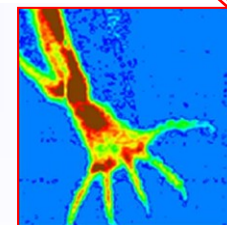
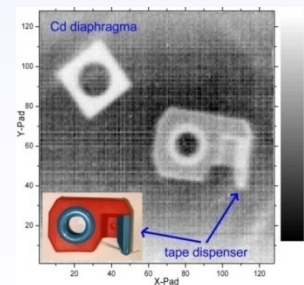
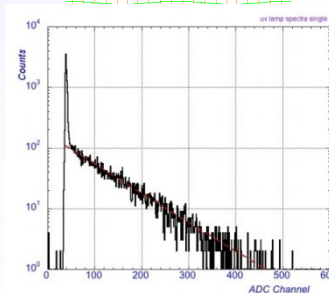
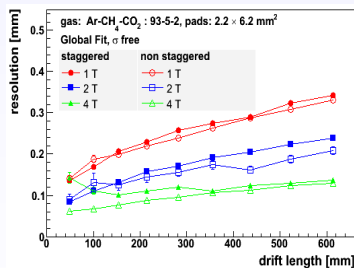
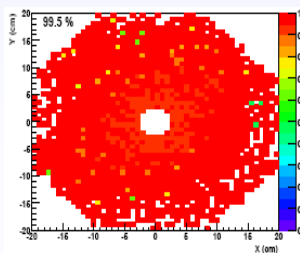
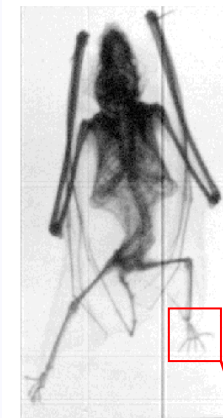
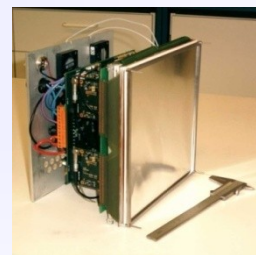
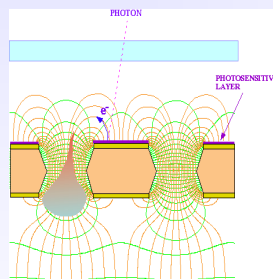
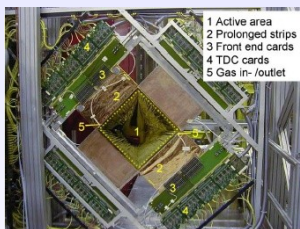
Efficiency decrease starts at same drift field with the data ($E_a/E_d \sim 55$)

- Predicted efficiency in the falling slope within 10% from the measurement

- ALICE:** TPC (tracker), TRD (transition rad.), TOF (MRPC), HMPID (RICH-pad chamber), Muon tracking (pad chamber), Muon trigger (RPC)
- ATLAS:** TRD (straw tubes), MDT (muon drift tubes), Muon trigger (RPC, thin gap chambers)
- CMS:** Muon detector (drift tubes, CSC), RPC (muon trigger)
- LHCb:** Tracker (straw tubes), Muon detector (MWPC, GEM)
- TOTEM:** Tracker & trigger (CSC , GEM)

Current Trends in Micro-Pattern Gas Detectors (Applications)

- High-Rate Particle Tracking and Triggering
- Time Projection Chamber Readout
- Photon Detectors for Cherenkov Imaging Counters
- X-Ray Astronomy
- Neutron Detection and Low Background Experiments
- Cryogenic Detectors
- Medical Applications
- Homeland Security and Prevention of Planetary Disasters



Tracking - Micromegas

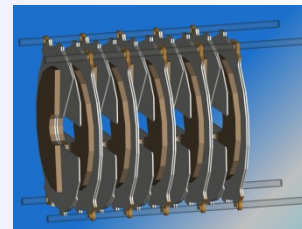
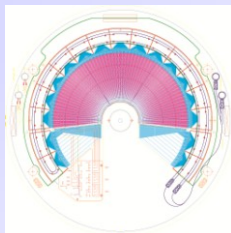
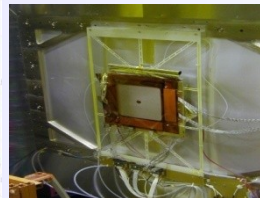
TPC readout - GEM

UV photon detection - GEM

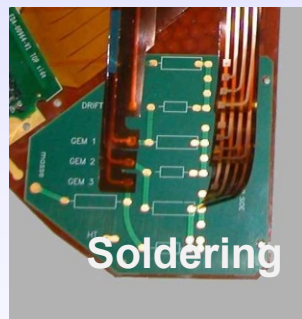
Neutron detection - GEM

Radiography - GEM

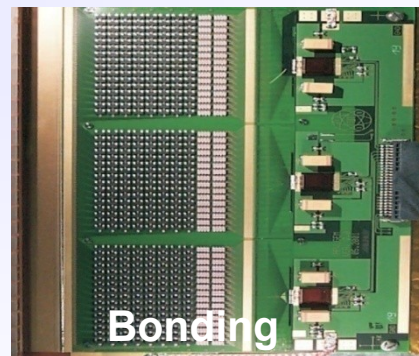
Detector Design



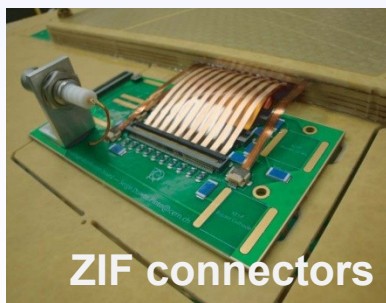
Services and Connectivity



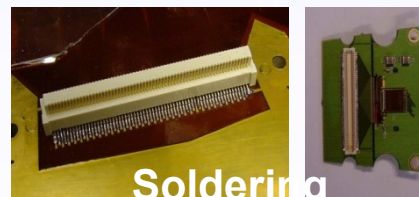
Soldering



Bonding

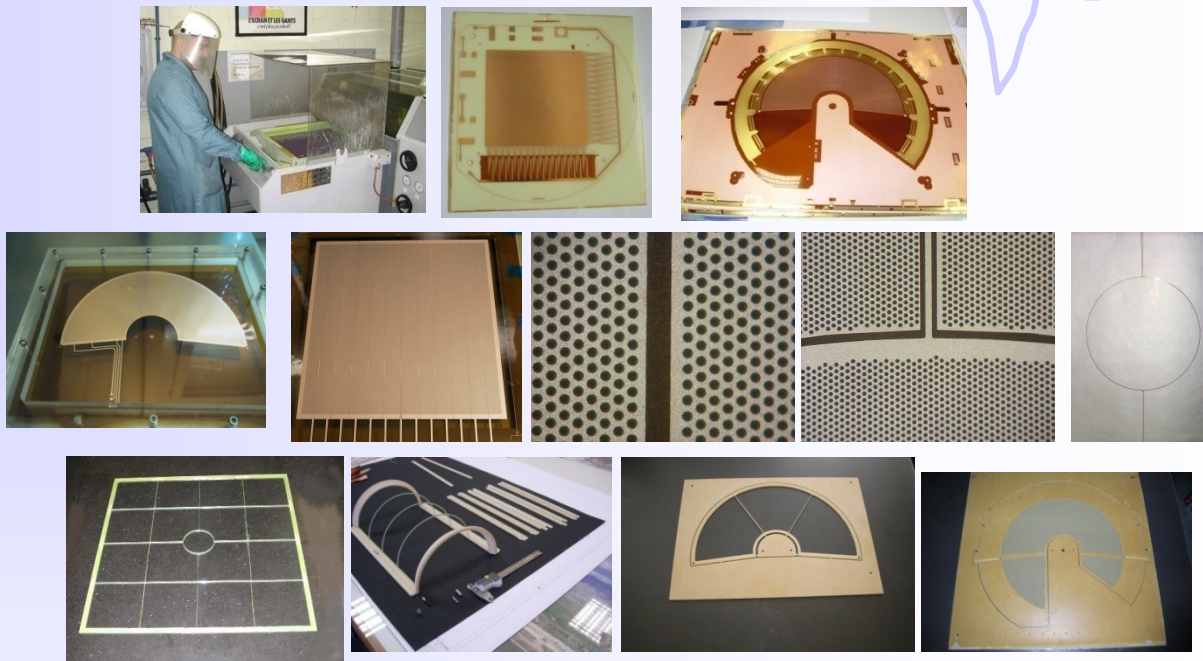


ZIF connectors



Soldering

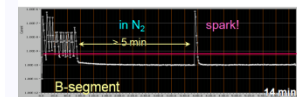
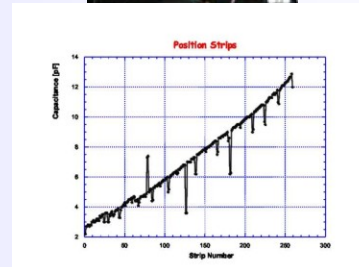
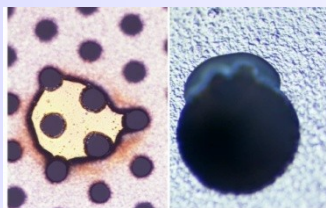
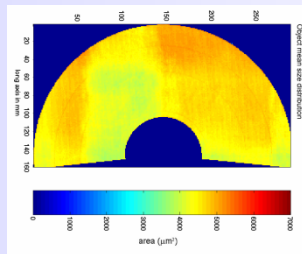
Component Production



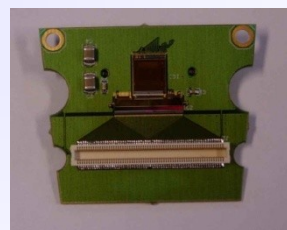
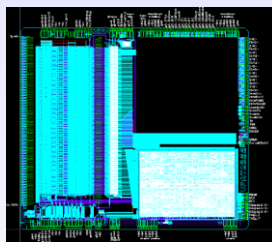
Infrastructure and Assembly Tools



Component Quality Control

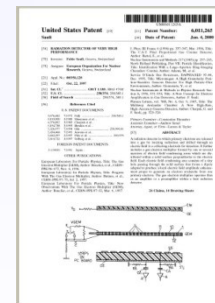


Electronics



APV
VFAT
GP5
ALTRO
MEDIPIX

Industrialization



PANalytical
3M
TechEtch
Techtra
Centronic
G&A

F. Sauli, IEEE Short Course on Radiation Detection and Measurement, Norfolk (Virginia)

November 10-11, 2002

C. Joram, CERN Academic Training, Particle Detectors 1998

P. Cwetanski , <http://pcwetans.home.cern.ch/pcwetans/>

M. Hoch, Trends and new developments in gaseous detectors, NIM A535(2004)1-15

Literature:

F. Sauli, Principles of operation of multiwire proportional and drift chambers, CERN 77-09

W. Blum and L. Rolandi, Particle Detection with Drift Chambers, Springer 1994

C. Grupen, Particle Detectors, Cambridge University Press, 1996

F. Sauli and A. Sharma, Micropattern Gaseous Detectors, Annu. Rev. Nucl. Part. Sci. 1999.49:341-88

<http://gdd.web.cern.ch/GDD/>